Article

An Innovative Applied Control System of Helicopter Turboshaft Engines Based on Neuro-Fuzzy Networks

Serhii Vladov [1,*], Oleksii Lytvynov [2], Victoria Vysotska [3,4], Viktor Vasylenko [1], Petro Pukach [5] and Myroslava Vovk [6,*]

[1] Kharkiv National University of Internal Affairs, 27, L. Landau Avenue, 61080 Kharkiv, Ukraine; vasylenko_viktor@ukr.net
[2] National Aerospace University "Kharkiv Aviation Institute", 17, Chkalova Street, 61070 Kharkiv, Ukraine; lytvynovalex@gmail.com
[3] Information Systems and Networks Department, Lviv Polytechnic National University, 12, Bandera Street, 79013 Lviv, Ukraine; victoria.a.vysotska@lpnu.ua or victoria.vysotska@uni-osnabrueck.de
[4] Institute of Computer Science, Osnabrück University, 1, Friedrich-Janssen-Street, 49076 Osnabrück, Germany
[5] Department of Computational Mathematics and Programming, Lviv Polytechnic National University, 12, Bandera Street, 79013 Lviv, Ukraine; petro.y.pukach@lpnu.ua
[6] Department of Mathematics, Lviv Polytechnic National University, 12, Bandera Street, 79013 Lviv, Ukraine
[*] Correspondence: serhii.vladov@univd.edu.ua (S.V.); myroslava.i.vovk@lpnu.ua (M.V.)

Abstract: This study focuses on helicopter turboshaft engine innovative fault-tolerant fuzzy automatic control system development to enhance safety and efficiency in various flight modes. Unlike traditional systems, the proposed automatic control system incorporates a fuzzy regulator with an adaptive control mechanism, allowing for dynamic fuel flow and blade pitch angle adjustment based on changing conditions. The scientific novelty lies in the helicopter turboshaft engines distinguishing separate models and the fuel metering unit, significantly improving control accuracy and adaptability to current flight conditions. During experimental research on the TV3-117 engine installed on the Mi-8MTV helicopter, a parametric modeling system was developed to simulate engine operation in real time and interact with higher-level systems. Innovation is evident in the creation of the failure model that accounts for dynamic changes and probabilistic characteristics, enabling the prediction of failures and minimizing their impact on the system. The results demonstrate high effectiveness for the proposed model, achieving an accuracy of 99.455%, while minimizing the loss function, confirming its reliability for practical application in dynamic flight conditions.

Keywords: helicopter turboshaft engines; adaptive control law; automatic control system; neuro-fuzzy network; control error

1. Introduction

1.1. The Relevance of the Research

The development and advancement of helicopter turboshaft engine (TE) control systems play a crucial role in modern aviation technology [1]. Helicopters operate in highly dynamic and variable environments, where ensuring optimal engine performance across all flight conditions requires sophisticated control strategies [2]. Traditional control laws [3–6], with fixed parameters, often fall short in addressing the complexity and variability seen during real-world operations, such as abrupt changes in altitude, air temperature, or engine load. There is a demand for adaptive systems that adjust engine parameters in real time, enhancing safety and efficiency.

Adaptive control laws offer a promising solution by dynamically adjusting control parameters based on real-time data, ensuring optimal engine performance under various conditions. This approach improves fuel efficiency, prolongs engine life, and reduces failure risks [7]. Mathematical modeling is critical in developing such systems, providing a

foundation for simulating engine behavior in diverse scenarios and allowing for fine-tuning before real-world application [8,9].

The latest innovations in artificial intelligence (AI) and machine learning bring new opportunities for enhancing adaptive control systems [10,11]. AI-driven methods enable more accurate predictions of engine behavior, allowing for better anticipation and mitigation of potential issues. These innovations pave the way for safer and more efficient helicopter operations, advancing aviation technology.

1.2. The State of the Art

In recent decades, numerous studies have focused on enhancing helicopter TE efficiency and reliability. The development of helicopter TE surrounding control algorithms relies on classical regulation approaches, such as PID controllers [12,13] and linear control models [14,15], which are commonly used in aviation. However, despite their effectiveness in static and predictable conditions, these systems often struggle with abrupt changes during operations, including sudden variations in load, altitude, or ambient temperature. Such limitations restrict their application in dynamic flight scenarios, particularly for helicopters that must quickly adapt to changing conditions.

Contemporary research has begun to concentrate on adaptive control systems capable of automatically modifying parameters in real time based on actual sensor data [16,17]. Examples include control methods utilizing Lyapunov's adaptive control theory [18], stabilizing engine performance under various deviations from normal operating conditions. The implementation of these systems has shown improvements in helicopter TE reliability and stability; however, challenges remain regarding the accuracy of predicting dynamic changes and accounting for random factors.

One promising direction involves applying machine learning methods [19,20] and artificial intelligence [10,11,21,22] to predict engine behavior while adapting control systems based on these predictions. Models based on neural networks [23–25] can predict engine performance across various modes, accumulating data for continuous learning, thereby enhancing management effectiveness. However, much research in this area focuses on isolated aspects, such as fault diagnosis or optimization in specific modes, rather than creating a comprehensive adaptive management system.

Based on the above, a new mathematical model for adaptive control law emerges as necessary, accounting for real-time changes in helicopter TE operating conditions. This model should utilize data gathered from onboard sensors, adjusting engine control parameters to maintain optimal performance. A critical aspect involves the mathematical modeling of processes occurring within the engine, enabling predictions regarding its behavior in unstable conditions and timely responses to changes.

Integrating artificial intelligence into this model will facilitate control adaptation and future system states' predictions based on the accumulated data. This approach will help anticipate failures, reduce component wear, and enhance overall reliability during helicopter operation. Implementing such technologies will represent a significant advancement in adaptive control systems, markedly improving safety and efficiency within aviation.

1.3. The Main Attributes of the Research

The ***object*** of the research is the helicopter TE control system. The ***research subject*** includes the developed helicopter TE control system methods and models. The ***research aim*** is to develop a helicopter TE fault-tolerant fuzzy automatic control system for maintaining stable performance despite malfunctions or anomalies in the system.

The following scientific and practical tasks were solved to achieve this aim:

1. The development of the proposed neural network system for predicting anomalous data in sensor systems;
2. The development of the helicopter TE adaptive control law;
3. The development of an intelligent automatic control system for the helicopter TE adaptive control law implementation;

4. The development of the fuzzy controller architecture and training algorithm;
5. The development of a semi-physical simulation stand for conducting computational experiments;
6. Conducting a computational experiment to evaluate helicopter TE control quality under conditions of actuator failure in the fuel flow control mechanism within the gas generator rotor r.p.m. channel.

The ***main contribution*** of the research is the development of the helicopter TE fault-tolerant fuzzy automatic control system, which enhances control accuracy and adaptability through a fuzzy regulator and adaptive mechanisms.

2. Materials and Methods

2.1. Development of Helicopter Turboshaft Engine Adaptive Control Law

Based on [26–28], the helicopter TE regulation law mathematical model, grounded in the present text, can be outlined as follows:

1. Engine (gas generator) operation is controlled by varying the fuel supply G_T. It is the sole parameter influencing the gas generator's operating mode, as the compressor is fixed, and the first stage of the accessible turbine functions as a throttle with a constant cross-section.
2. Maintaining constant free turbine speed n_{FT} = const is key for safe helicopter piloting. To meet this condition, the automatic control system (ACS) adjusts G_T when the blade pitch angle of the main rotor $\varphi_{m.r.}$ changes.
3. The control model is expressed as follows:

   - n_{FT} = const, if $\varphi_{m.r.} \leq \varphi_{m.r.\max}$;
   - If $\varphi_{m.r.} > \varphi_{m.r.\max}$, the ACS limits fuel supply, and n_{FT} starts to decrease to constrain one of the limiting parameters (e.g., maximum turbine speed $n_{TC\max}$ or maximum power N_e).

4. The free turbine rotor speed regulator central equation when the fuel supply changes is as follows:

$$n_{FT} = f(G_T, \varphi_{m.r.}, n_{TC}, N_e). \tag{1}$$

5. The power limitation condition is represented as follows:

$$N_e \leq N_e^{\max}. \tag{2}$$

6. Upon reaching the maximum power limit $N_e = N_e^{\max}$, maintaining n_{FT} = const becomes impossible, and the n_{FT} frequency decreases.

The central regulation equation for the free turbine while maintaining the rotational frequency n_{FT} can be expressed through the power balance:

$$N_{FT} = N_{m.r.} + N_{power\ loss}. \tag{3}$$

The free turbine power is expressed as follows:

$$N_{FT} = \eta_{FT} \cdot \frac{G_T \cdot \dot{Q}}{c_p \cdot T_G^*}, \tag{4}$$

where $\dot{Q} = G_T \cdot H_u$.

The variation in fuel supply based on the rotational frequency of the free turbine and required power is defined by the following expression:

$$G_T = \frac{n_{FT}^2 \cdot N_{m.r.}}{\eta_{FT} \cdot H_u \cdot c_p \cdot T_G^*}. \tag{5}$$

Thrust control for the main rotor through the blade pitch angle is performed according to the following equation:

$$T_{m.r.} = C_T(\varphi_{m.r.}) \cdot \rho \cdot n_{FT}^2 \cdot A_{m.r.}. \tag{6}$$

The control relations for the blade pitch angle are represented as follows:

$$\varphi_{m.r.} = f(T_{m.r.}, H, P_a, T_a). \tag{7}$$

Considering changes in altitude and ambient temperature, correction factors for fuel flow are introduced:

$$G_T(H, T_a) = G_T \cdot \left(1 + k_H \cdot \frac{H}{H_{max}}\right) \cdot \left(1 + k_T \cdot \frac{T_a - T_N}{T_N}\right). \tag{8}$$

To ensure safe operation, restrictions are introduced on parameters such as maximum power N_e, gas generator rotor r.p.m. $n_{TC\max}$, and the gas temperature in the front of the turbine $T_G^{*\max}$ [29,30]:

$$\begin{aligned} N_e &= N_e^{\max}, \\ n_{TC} &\leq n_{TC\max}, \\ T_G^* &\leq T_G^{*\max}. \end{aligned} \tag{9}$$

If any restriction is reached, the system adjusts fuel flow G_T to maintain engine operation within safe values:

$$G_T = \min\left(G_T, G_T^{lim}\right). \tag{10}$$

To ensure effective system operation across different flight modes, an adaptive control law is introduced which adjusts parameters based on the current power N_e and frequency n_{FT}:

$$G_T = G_T^{base} \cdot \left(1 + \alpha \cdot \frac{N_e - N_e^{req}}{N_e^{req}}\right) \cdot \left(1 + \beta \cdot \frac{n_{FT} - n_{FT}^{req}}{n_{FT}^{req}}\right). \tag{11}$$

By combining all equations, a general control law is obtained:

$$\varphi_{m.r.} = f(T_{m.r.}, \varphi_{m.r.}, H, P_a, T_a, T_G^*). \tag{12}$$

To develop a mathematical model for the control law numerical solution in the "pitch-throttle" system for helicopter TEs, employing numerical optimization methods and discretization of the differential equation system describing engine dynamics proves effective [31,32]. The "pitch-throttle" system [33] regulates fuel flow and the angle of attack of the main rotor blades to maintain the free turbine, which requires rotational frequency n_{FT}, power N_e, and rotor thrust $T_{m.r.}$. The free turbine rotational frequency n_{FT} depends on fuel flow and the main rotor resistance torque. In differential form, the equation can be expressed as follows:

$$J_{FT} \cdot \frac{dn_{FT}(t)}{dt} = M_{FT}(t) - M_{m.r.}(t). \tag{13}$$

The free turbine moment $M_{FT}(t)$ depends on fuel flow $G_T(t)$ and gas temperature T_G^*:

$$M_{FT}(t) = \eta_{FT} \cdot \frac{G_T(t) \cdot H_u}{c_p \cdot T_G^*(t)}. \tag{14}$$

The main rotor thrust $T_{m.r.}(t)$ depends on the blade pitch angle $\varphi_{m.r.}(t)$ and the free turbine speed $n_{FT}(t)$:

$$T_{m.r.}(t) = C_T(\varphi_{m.r.}(t)) \cdot \rho(t) \cdot n_{FT}^2(t) \cdot A_{m.r.}. \tag{15}$$

For numerical solutions, the Euler method is applied for time integration with a time discretization step Δt [34]. The discretized equation for free turbine speed is defined as follows:

$$n_{FT}(t + \Delta t) = n_{FT}(t) + \frac{\Delta t}{J_{FT}} \cdot (M_{FT}(t) - T_{m.r.}(t)). \tag{16}$$

To ensure numerical stability, the time step Δt must satisfy a stability condition. Specifically, Δt should be less than a certain threshold determined by the system's dynamic properties, such as the inertial moment J_{FT} and the maximum expected rate of the torque difference $(M_{FT} - T_{m.r.})$ change. For stability, a common guideline is $\Delta t < \frac{J_{FT}}{\max\left|\frac{d(M_{FT}(t) - T_{m.r.}(t))}{dt}\right|}$.

The discretized equation for the main rotor thrust takes the following form:

$$T_{m.r.}(t + \Delta t) = C_T(\varphi_{m.r.}(t)) \cdot \rho(t) \cdot n_{FT}^2(t + \Delta t) \cdot A_{m.r.}. \tag{17}$$

2.2. The Development of the Algorithm for the Discretized Equation for the Main Rotor Thrust Numerical Solution

An algorithm for the numerical solution is proposed, consisting of the following steps:

1. Initialization of the initial conditions as follows:

$$n_{FT}(0) = n_{FT0}, \, \varphi_{m.r.}(0) = \varphi_{m.r.0}, \, G_T(0) = G_{T0}, \, H(0) = H_0, \, T_a(0) = T_{a0}. \tag{18}$$

2. Computation is performed at each time step:
    *   Fuel flow $G_T(t)$ and the blade pitch angle $\varphi_{m.r.}(t)$ are updated according to the "pitch-throttle" system control law based on the specified target parameters n_{FT}^{req} and $T_{m.r.}^{req}$.
    *   The free turbine rotor speed $n_{FT}(t + \Delta t)$ is calculated.
    *   The thrust $T_{m.r.}(t + \Delta t)$ is calculated.
    *   External parameters $H(t + \Delta t)$, $T_a(t + \Delta t)$, and $P_a(t + \Delta t)$ are updated.

3. Deviations are assessed. Deviations in turbine speed and thrust from target values are calculated according to the following expression:

$$\Delta n_{FT}(t) = n_{FT}(t) - n_{FT}^{req}, \, \Delta T_{m.r.}(t) = T_{m.r.}(t) - T_{m.r.}^{req}. \tag{19}$$

4. Control signals are adjusted as follows:
    *   If $|\Delta n_{FT}(t)| > \varepsilon_n$, then then fuel flow $G_T(t)$ is adjusted.
    *   If $|\Delta n_{FT}(t)| > \varepsilon_T$, then the blade pitch angle $\varphi_{m.r.}(t)$ is adjusted.

5. Transition to the next time step is carried out according to the following expression:

$$t \leftarrow t + \Delta t. \tag{20}$$

Based on the above, the proposed adaptive control law for fuel flow and the blade pitch angle involves adjusting fuel flow $G_T(t)$ and the pitch angle $\varphi_{m.r.}(t)$ according to deviations in rotational speed and thrust:

$$\begin{aligned} G_T(t + \Delta t) &= G_T(t) + k_G \cdot \Delta n_{FT}(t), \\ \varphi_{m.r.}(t + \Delta t) &= \varphi_{m.r.}(t) + k_\varphi \cdot \Delta T_{m.r.}(t). \end{aligned} \tag{21}$$

The system continues integration until the deviations in rotational speed n_{FT} and thrust $T_{m.r.}$ become less than the specified tolerances ε_n and ε_T:

$$|\Delta n_{FT}(t)| \leq \varepsilon_n, \, |\Delta n_{FT}(t)| \leq \varepsilon_T. \tag{22}$$

The proposed model employs numerical solutions to solve the differential equation system that describes the helicopter TE dynamics and the rotor blades. The system enables

real-time numerical solutions for regulating fuel flow and the blade pitch angle through the discretization of equations and the Euler method.

In the research's next stage, the helicopter TE control program in limitation modes is developed. To achieve this, the following aspects must be considered:

1. Determining limiting modes by establishing a limiting-mode line. This is based on the relations between the maximum allowable values for the parameter n_{TC}^{given} and temperature at the input to the gas generator (in this case, temperature T_N).

2. Establishing the dependence on temperature through the expression $\left(n_{TC}^{given}\right)_{lim} = f(T_N)$ [31], which includes segments (Figure 1) 1–2 for $\left(n_{TC}^{given}\right)_{max}$; 2–3 for $n_{TC\max}$; and 3–4 for another limiting parameter (for example, limitations on power N_e).

3. Identifying areas of limitation modes based on changes in temperature T_N. In this case, three areas are distinguished (Figure 2) [31]:

   - At low values of T_N (for example, $T_N < T_{N2}$), a limitation on $\Delta K_{y\min}$ is observed.
   - In the temperature range from T_{N2} to T_{N3}, a limitation on $n_{TC\max}$ must be maintained.
   - When $T_N > T_{N3}$, a limitation on another limiting parameter takes effect.

4. Additional limitations involve adding a power limitation line $N_e^{\max}$ to the limiting-mode line, resulting in a structure consisting of four segments that account for all constraints. In this case, equations describing the relations between power N_e, engine parameters, and temperature are represented by (9).

5. Under limitation conditions, the proposed control program forms an equation system linking fuel supply G_T, blade pitch angle $\varphi_{m.r.}$, and power parameters, presented in (11).
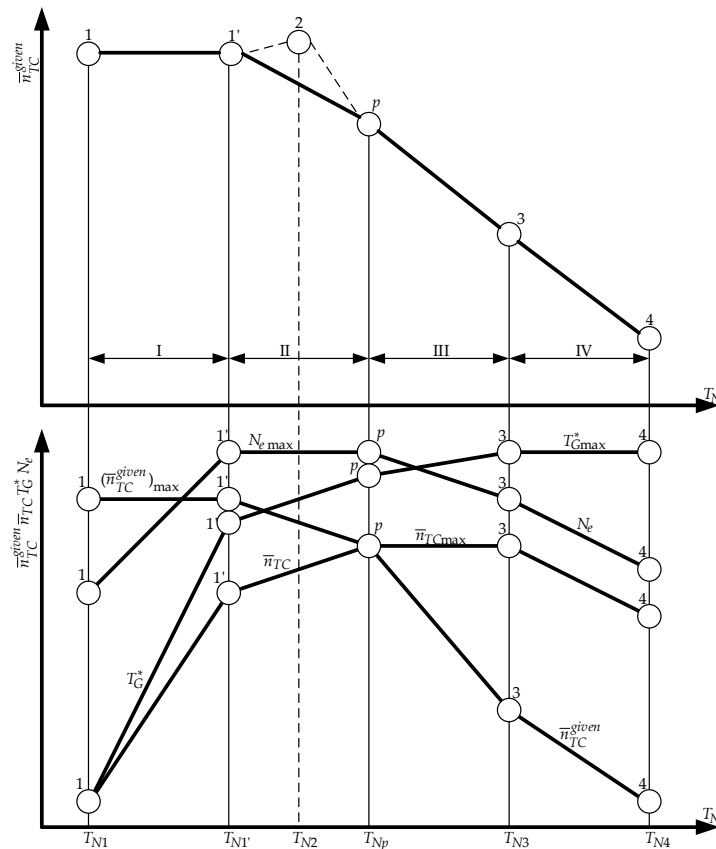

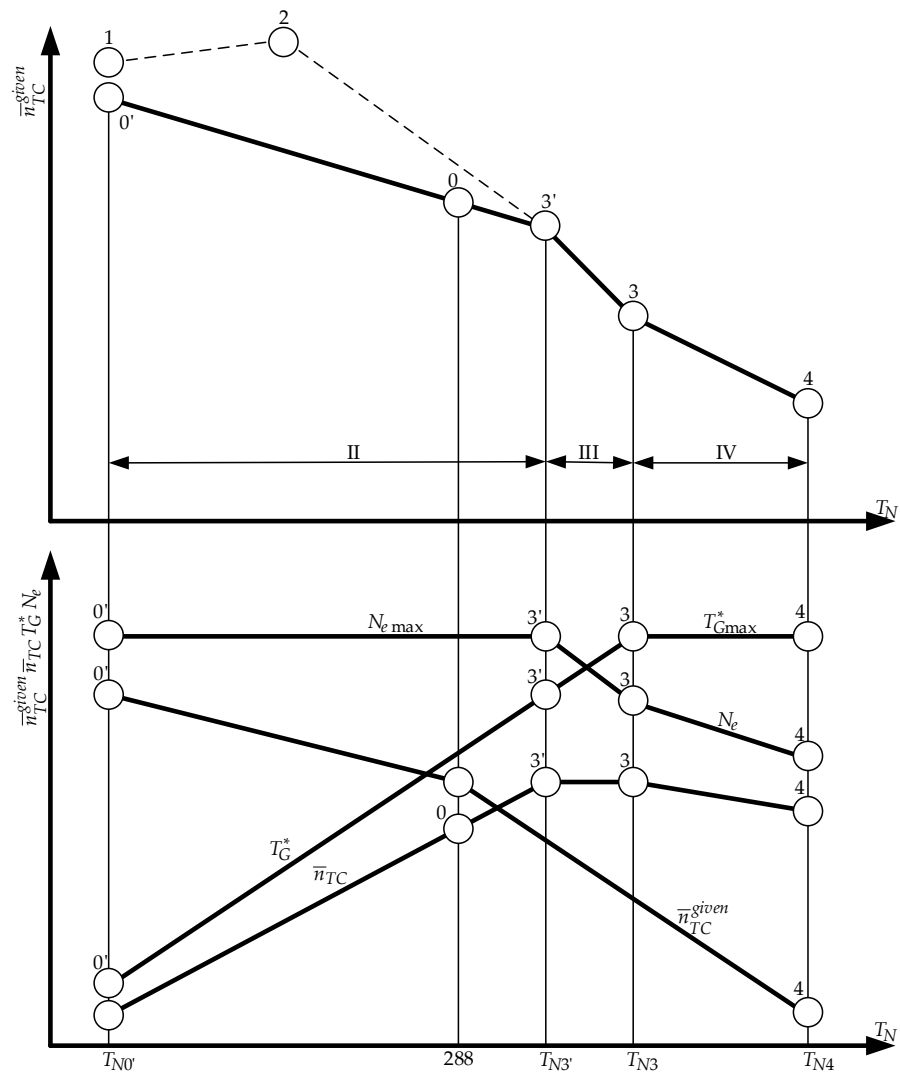**Figure 1.** The limiting-mode line.

Figure 2. The limiting-mode line.

Thus, the developed helicopter TE control adaptive mathematical model is presented as follows:

$$\left(n_{TC}^{given}\right)_{lim} = f(T_N),$$
$$G_T = G_T^{base} + k_G \cdot \Delta n_{FT}(t),$$
$$\varphi_{m.r.}(t + \Delta t) = \varphi_{m.r.}(t) + k_\varphi \cdot \Delta T_{m.r.}(t),$$
$$N_e = N_e^{\max}, \; n_{TC} \leq n_{TC\max}, \; T_G^* \leq T_G^{*\max}. \tag{23}$$

The innovative aspect lies in the developed helicopter TE adaptive control law that enhances performance and safety compared to traditional control systems [35–40]. This adaptive approach dynamically adjusts fuel supply and blade pitch angle based on real-time conditions, ensuring constant free turbine rotor speed and optimal engine operation under varying flight parameters. Unlike conventional methods that rely on fixed settings, the proposed model integrates real-time feedback to maintain safe operational limits, addressing constraints such as maximum power, gas generator rotor r.p.m., and gas temperature. The model facilitates real-time regulation by employing numerical optimization techniques and discretizing differential equations, improving responsiveness and efficiency in diverse flight modes, thus significantly advancing the helicopter TE control system's capabilities. The developed model is presented in Figure 3.
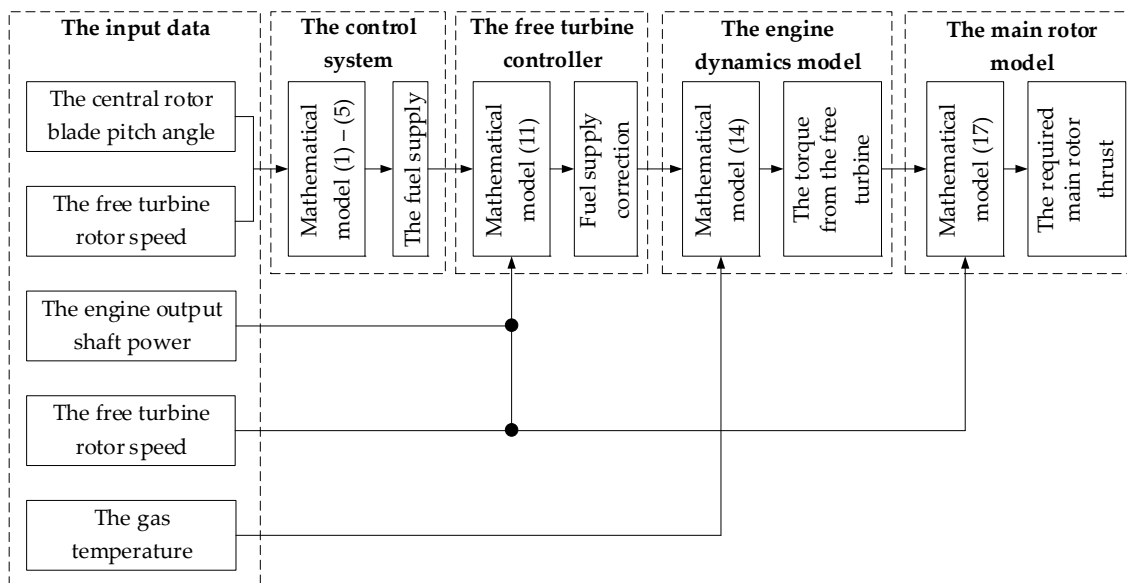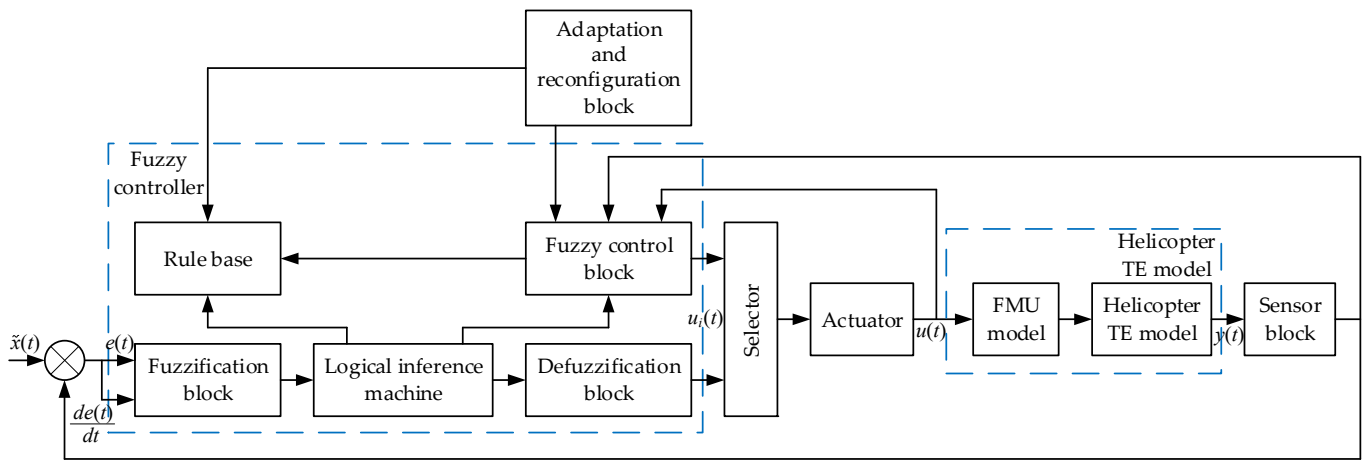
Figure 3. The proposed helicopter turboshaft engine fuzzy fault-tolerant control system.

2.3. The Development of an Intelligent Automatic Control System for the Implementation of the Helicopter Turboshaft Engine Adaptive Control Law

The research proposes a helicopter TE fuzzy fault-tolerant control system (FTCS) (Figure 4) aimed at implementing the developed control law (23). Traditional control systems [35–37] are often based on linear models that fail to account for nonlinear engine dynamics, resulting in reduced efficiency and increased risk under changing external conditions. Systems built on classical neural networks provide better adaptability [38–43], but they lack interpretability, may struggle with uncertainty, require extensive training datasets, and are prone to overfitting. Neuro-fuzzy control systems based on adaptive neuro-fuzzy inference systems (ANFISs) [44–46] combine the strengths of fuzzy logic and neural networks, allowing for the processing of fuzzy data and the integration of expert knowledge. However, they may require retraining during rapid changes in conditions. On the other hand, neuro-fuzzy systems based on adaptive neural networks (AFNNs) [47] offer more powerful control strategies and quickly adapt to changes, although their implementation demands significant computational resources. A comparison of different systems shows that the FTCS is the most appropriate choice for implementing the developed helicopter TE control law (23), combining adaptability, interpretability, and the ability to handle uncertainty, thus enhancing the reliability, safety, and performance of the helicopter TE compared to traditional systems and those based on neural networks and ANFISs. Traditional systems based on linear models do not take into account the nonlinear dynamics of the engine, which reduces efficiency and increases risks when external conditions change. Systems based on classical neural networks provide better adaptability, but are inferior in interpretability and resistance to uncertainty. The proposed FTCS based on ANFISs or AFNNs combines neural networks and fuzzy logic advantages, which makes it the optimal choice for helicopter TE control due to the ability to adapt to changes, process uncertainty, and increase reliability.

The proposed helicopter TE FTCS (Figure 4) consists of a fuzzy controller, an adaptation and reconfiguration module, a selector of engine parameters in control channels, an actuator block, an engine model, a fuel metering unit (FMU) model, and a sensor block for the measured parameters. The fuzzy controller, in turn, comprises a fuzzification block, an inference engine, a defuzzification unit, a fuzzy rule base, and a fuzzy control block. A key distinction of the proposed FTCS compared to the closest analogue [48] is the division of the engine model into the engine model itself and the FMU model, first introduced in [38,41,42]. It allows for more precise consideration of the interaction between the engine and the metering needle, improving control accuracy and adaptation to changing operat-

ing conditions [41,42]. This approach provides better control of operational parameters, enhancing overall system efficiency and reducing the likelihood of emergencies.

Figure 4. The proposed helicopter turboshaft engine fuzzy fault-tolerant control system.

Furthermore, the model division [38,40–42] enables more efficient integration of expert knowledge into the control process, further enhancing the system's flexibility and adaptability and ensuring high resilience to uncertainty and external influences. The proposed FTCS fault-tolerant system has the ability to adapt to changing operating conditions and maintain stable performance in the presence of uncertainty and external impacts. The adaptation and reconfiguration modules and the division into the engine and FMU models enable the system to respond quickly to malfunctions and ensure safe control, minimizing the risk of emergencies.

For the fuzzification of input values, for example, the input variable x is transformed into fuzzy values $\widetilde{x}$ using membership functions $\mu_A(x)$ [46,49–51]:

$$
\begin{aligned}
\widetilde{x} &= (A_1, A_2, \ldots, A_n), \\
\mu_A(x) &= \exp\left(-\frac{(x-c_i)^2}{2\cdot\sigma_i^2}\right).
\end{aligned}
\tag{24}
$$

Based on the fuzzy rules defined in the rule base, inference is performed using a logic inference engine. If a rule has the form

$$
\text{IF } x \text{ is } A_i, \text{ THEN } y = f_i(x),
\tag{25}
$$

then the rule activation can be represented as follows:

$$
w_j = \min\left(\mu_{A_i}(x)\right).
\tag{26}
$$

To obtain an accurate output value y, a defuzzification method such as the modified center of gravity, developed in [45], is used:

$$
y = \frac{\sum_j w_j \cdot y_j \cdot \mu_j(x)}{\sum_j w_j \cdot \mu_j(x)},
\tag{27}
$$

where y_j represents category A_j, $\sum_j w_j \cdot y_j \cdot \mu_j(u)$ is the weighted sum of category centers and their membership degrees, and $\sum_j w_j \cdot \mu_j(u)$ is the sum of the membership-weighted degrees [45]. In the traditional gravity method's equation for the center, $y = \frac{\sum_j y_j \cdot \mu_j(x)}{\sum_j \mu_j(x)}$, all fuzzy inference points are treated with equal weight, which can result in underestimating or overestimating specific categories. For instance, if one category has greater significance than another, this could skew the defuzzification outcome. The modified equation in (27) allows

each category's degree of importance to be considered during defuzzification, enhancing inference precision while incorporating the weighting coefficient's influence on the result. It is noted in [45] that the gravity method with a modified center and weights outperforms the traditional approach, as it allows for a more accurate representation of each membership category's significance in the final value. It is beneficial in cases where specific categories have a more substantial influence or higher importance than others.

The adaptation block is described using dynamic equations of the following form:

$$\frac{d\theta}{dt} = \mu \cdot \gamma \cdot (y_{desired} - y_{actual}). \tag{28}$$

The helicopter TE dynamics can be described using differential equations [52]. For example, the state equation can be represented as follows:

$$\frac{dP}{dt} = f(n_{TC}, n_{FT}, T_G^*, \delta) + \omega. \tag{29}$$

The FMU operation is described by an equation of the following form [52]:

$$\frac{dD}{dt} = k \cdot (D_{desired} - D_{actual}) + c \cdot D. \tag{30}$$

Actuators can be described by a regulator equation related to the system output parameters. For example [53,54],

$$u(t) = K_p \cdot e(t) + K_i \cdot \int_0^t e(\tau) d\tau + K_d \cdot \frac{de(t)}{dt}. \tag{31}$$

The proportional term $K_p \cdot e(t)$ delivers an immediate reaction to the error, while the integral term $K_i \cdot \int_0^t e(\tau) d\tau$ accounts for the cumulative errors over time. The differential term $K_d \cdot \frac{de(t)}{dt}$ mitigates overshoot by making adjustments based on the change rate in the error [53].

Sensor signals are represented as follows [38,41,42]:

$$S = h(n_{TC}, n_{FT}, T_G^*, \delta) + \epsilon. \tag{32}$$

Thus, Expressions (28)–(32) form the overall helicopter TE FFCS model.

2.4. Development of Fuzzy Controller

The research proposes the implementation of a fuzzy controller using a fuzzy neural network (Figure 5) for the developed control law (23) by structuring the model with fuzzification, inference, and defuzzification components, integrating the provided specific control laws. The fuzzy controller now takes the control error $e(t)$ and the error change rate $\frac{de(t)}{dt}$ as input parameters; the output is the control action $u(t)$. This structure includes the fuzzification block, converting the control error $e(t)$ and its change rate $\frac{de(t)}{dt}$ into fuzzy values. An inference machine uses fuzzy rules to derive the appropriate control action based on the inputs. The defuzzification block converts the fuzzy output into a crisp control action. A fuzzy rule base contains rules linking $e(t)$ and $\frac{de(t)}{dt}$ to the control output $u(t)$. The control law implements the control action according to the provided control law.
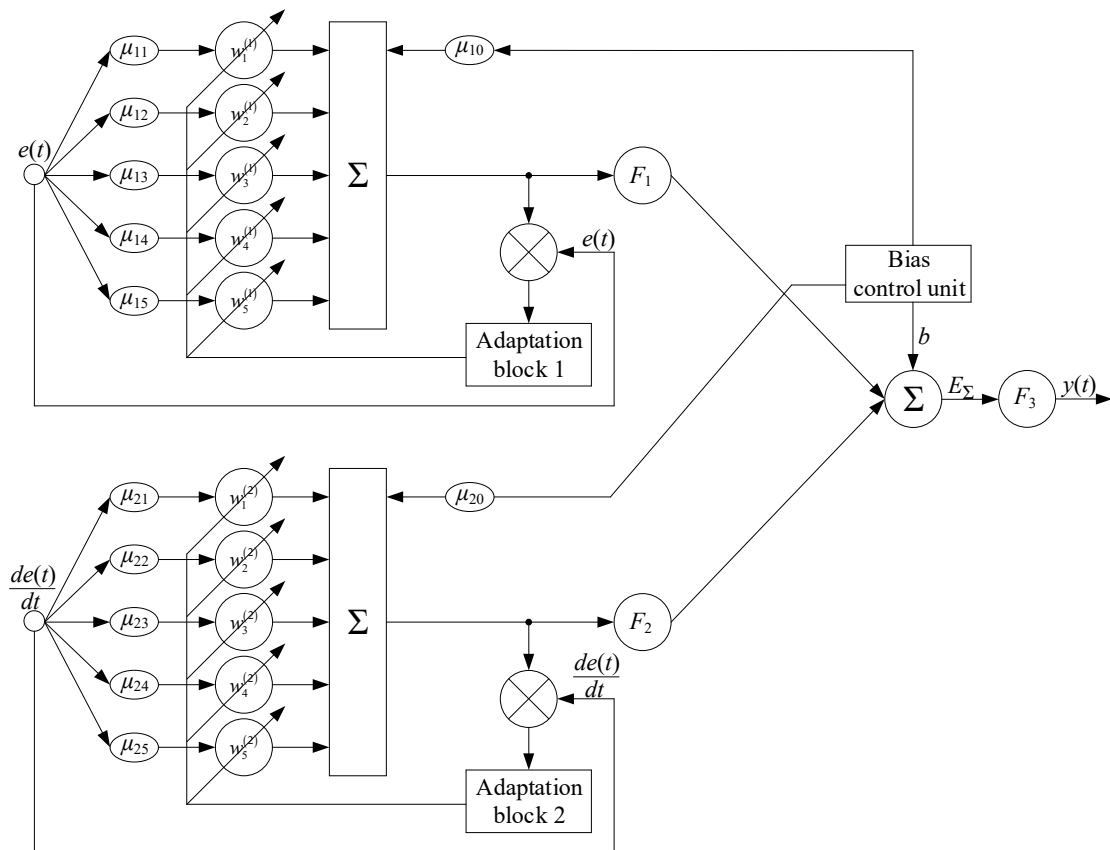
Figure 5. The fuzzy controller scheme implemented as a fuzzy neural network.

The input parameters are as follows:

1. The control error is calculated as

$$e(t) = e_{n_{TC}} + e_{n_{FT}} + e_{T_G^*} + e_{T_N} + \ldots, \tag{33}$$

where $e_{n_{TC}} = n_{TC}^{given} - n_{TC}(t)$, $e_{n_{FT}} = n_{FT}^{given} - n_{FT}(t)$, $e_{T_G^*} = T_G^{*given} - T_G^*(t)$. It is noted that the components in (33) may vary depending on the input data amount.

2. The error change rate $\frac{de(t)}{dt}$.

The fuzzification process converts these inputs into fuzzy values using membership functions, i.e.,

$$\mu_e(e(t)) = \exp\left(-\frac{\left(e(t) - c_{e(t)}\right)^2}{2 \cdot \sigma_{e(t)}^2}\right),$$

$$\mu_{\frac{de(t)}{dt}}\left(\frac{de(t)}{dt}\right) = \exp\left(-\frac{\left(\frac{de(t)}{dt} - c_{\frac{de(t)}{dt}}\right)^2}{2 \cdot \sigma_{\frac{de(t)}{dt}}^2}\right). \tag{34}$$

The inference machine applies fuzzy rules to the fuzzified inputs $\widetilde{e}(t)$ and $\frac{d\widetilde{e}(t)}{dt}$ to determine the control action. The fuzzy rule base can be written as follows:

$$\begin{aligned}
&\text{Rule 1: If } e(t) \text{ is "negative large" and } \tfrac{de(t)}{dt} \text{ is "negative large", then } u(t) \text{ is "large positive".} \\
&\text{Rule 2: If } e(t) \text{ is "small" and } \tfrac{de(t)}{dt} \text{ is "zero", then } u(t) \text{ is "zero".}
\end{aligned} \tag{35}$$

The inference process is performed using a fuzzy logic operator (e.g., minimum or product rule):

$$\mu_{out}(u(t)) = \min\left(\mu_e(e(t)), \mu_{\frac{de(t)}{dt}}\left(\frac{de(t)}{dt}\right)\right). \tag{36}$$

Expression (36) gives the fuzzy output membership function for the control action $u(t)$. Defuzzification converts the fuzzy output into a crisp control value using (27). The fuzzy rule base is constructed to link the control error $e(t)$ and its change rate $\frac{de(t)}{dt}$ to the control action $u(t)$. The rules define how the control system should respond to different combinations of $e(t)$ and $\frac{de(t)}{dt}$. Example rules include the following:

$$\begin{aligned} &\text{Rule 1}: \text{ If } e(t) \text{ is "positive large" and } \tfrac{de(t)}{dt} \text{ is "positive small", then } u(t) \text{ is "decrease".}\\ &\text{Rule 2}: \text{ If } e(t) \text{ is "negative small" and } \tfrac{de(t)}{dt} \text{ is "negative large", then } u(t) \text{ is "increase".} \end{aligned} \tag{37}$$

The fuzzy control action is used to regulate system parameters according to the given control law (23). Examples are given below:

1. $\left(n_{TC}^{given}\right)_{lim} = f(T_N)$. This control law uses the error in gas generator rotor r.p.m. $e_{n_{TC}} = n_{TC}^{given} - n_{TC}(t)$ as one of the inputs.

2. $G_T = G_T^{base} + k_G \cdot \Delta n_{FT}(t)$. It can be controlled based on the fuzzy output $u(t)$, where u(t) affects $\Delta n_{FT}(t)$, the change in free turbine speed.

3. $\varphi_{m.r.}(t + \Delta t) = \varphi_{m.r.}(t) + k_\varphi \cdot \Delta T_{m.r.}(t)$, where the control action $u(t)$ determines the adjustment to the rotational speed $\varphi_{m.r.}(t)$.

4. The control actions must also satisfy the constraints given in the system $N_e = N_e^{max}$, $\underline{n_{TC}} \le \underline{n_{TC}}_{max}$, $T_G^* \le T_G^{*max}$.

The fuzzy neural network ensures that the control actions adhere to these limits by adjusting $u(t)$ accordingly.

The final control action $u(t)$ is computed based on the fuzzified error $e(t)$ and error change rate $\frac{de(t)}{dt}$ passed through the inference machine and defuzzification block. The result is a crisp value that modifies the system parameters in real time:

$$u(t) = \{\textit{Defuzzified output from fuzzy controller}\}. \tag{38}$$

This fuzzy neural network design allows for the adaptive control of the helicopter TE parameters based on the error and error change rate, ensuring robust performance across different operating conditions.

Fault tolerance is assessed by the system's ability to correctly compensate for the impact of failures on control and engine performance. A corrective control signal $u_c(t)$ is generated based on fuzzy adaptation rules in the event that failures occur:

$$u(t) = u_0(t) + u_c(t). \tag{39}$$

It is assumed that $d(t)$ is a failure vector, which is described through binary failure indicators (for example, sensor failure, drive failure):

$$d(t) = [d_1(t), d_2(t), \ldots, d_k(t)]^T \tag{40}$$

where $d_i(t)$ takes the value 1 in the case of failure and 0 in the case of regular operation.

A cost function J is introduced to evaluate system deviations from the target values:

$$J = \int_0^T \left\|x(t) - x_{ref}(t)\right\|^2 + \gamma_1 \cdot \|u(t)\|^2 + \gamma_2 \cdot \|d(t)\|^2 dt. \tag{41}$$

The system is considered fault-tolerant if $J \le J_{max}$, where J_{max} is the maximum permissible deviation level. After failure, the system applies an iterative recovery process,

minimizing the cost function *J*. Each iteration of correction takes the current failure vector $d(t)$ into account and updates the corrective control signal $u_c(t)$, i.e.,

$$u_c^{(k+1)} = u_c^{(k+1)} - \gamma \cdot \frac{\partial J}{\partial u_c}. \tag{42}$$

The proposed fault tolerance mathematical model in the helicopter TE fuzzy control system enables the simulation of failure impacts and adaptive control strategies to minimize their effects. Based on fuzzy logic, the system dynamically adjusts control actions, ensuring the stability and reliability of engine operation in real time.

3. Results

3.1. Input Data Preprocessing

The software product Matlab 2014b was used to conduct the computational experiment in the research. For the computational experiment, the aviation engine TV3-117 was selected as the research object, which is part of the powerplant for the Mi-8MTV helicopter [55,56]. The parameters of the TV3-117 engine (n_{TC}, n_{FT}, T_G^*, etc.) required for the computational experiment were derived solely from flight data recorded during the testing of the Mi-8MTV helicopter. Data registration was performed onboard using D-2M and D-1M sensors, along with 14 paired thermocouples T-101 [51] (data recording occurred over a 320 s interval during an actual flight with a sampling period of 1 s). These data were provided upon an official request from the authors' team to the Ministry of Internal Affairs of Ukraine and are intended for implementation in the project "Theoretical and Applied Aspects of Aviation Development", officially registered in Ukraine under number 0123U104884. The variation in parameters for the TV3-117 engine illustrates the complexity of the time series (Figure 6) [57], and the diagrams indicate the need to account for the current values of the parameters and the accumulation of data in the model's memory [58,59]. Figure 6 shows an increase in the parameters within the interval from 21 to 62 s of approximately 1.5 to 1.8 times due to the engine's transitional operating mode. As mentioned in the Introduction, the engine operates in steady modes about 85% of the time and only about 15% in transitional modes. Following [40–42,45–47,51,54], 256 values for n_{TC}, n_{FT}, T_G^*, etc., were selected, as illustrated in Figure 6. Based on the parameters n_{TC}, n_{FT}, T_G^*, etc., the selected values, the control error values, and the control error rate are obtained (Table 1), constituting the training dataset.
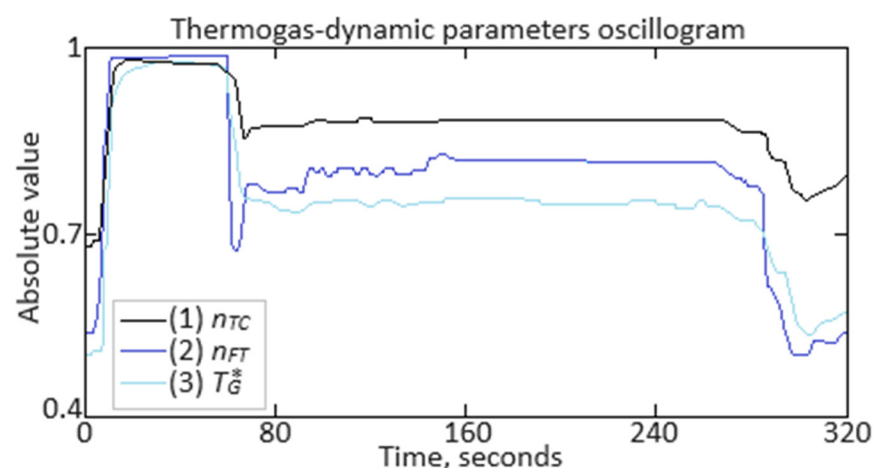
Figure 6. The TV3-117 turboshaft engine parameters in a dynamic time series using digitized oscillograms: the black curve is the gas generator rotor r.p.m; the violet curve is the free turbine rotor speed; the light blue curve is the gas temperature in the front of the compressor turbine.

Table 1. The training dataset fragment.

Number	1	...	38	...	84	...	127	...	181	...	219	...	256
$e(t)$	0.008	...	0.005	...	0.003	...	0.007	...	0.006	...	0.006	...	0.006
$\frac{de(t)}{dt}$	0.017	...	0.012	...	0.013	...	0.018	...	0.014	...	0.014	...	0.014

The training dataset homogeneity was assessed according to the Fisher–Pearson [60–62] and Fisher–Snedecor [63–65] criteria at a significance level of $\alpha = 0.01$ (Table 2). The significance level of 0.01 was chosen in the control task for helicopter gas turbine engines to ensure high reliability in statistical conclusions, which is particularly crucial in aviation safety. This stringent criterion minimizes type I error likelihood, contributing to more accurate and safer engine control across various operating modes.

Table 2. The training dataset homogeneity evaluation results for parameters $e(t)$ and $\frac{de(t)}{dt}$.

Parameter	Criterion Meaning		Description
	Calculated	Critical	
The Fisher–Pearson criterion			
$e(t)$	6.318	6.6	The Fisher–Pearson criterion yielded values for each parameter $e(t)$ and $\frac{de(t)}{dt}$ that fell below the
$\frac{de(t)}{dt}$	6.327		critical threshold, signifying homogeneity within the training dataset.
The Fisher–Snedecor criterion			
$e(t)$	2.388	2.58	The Fisher–Snedecor criterion produced values for each parameter $e(t)$ and $\frac{de(t)}{dt}$ that were
$\frac{de(t)}{dt}$	2.394		below the critical threshold, suggesting homogeneity within the training dataset.

The training and test datasets' representativeness was assessed through cluster analysis, which involved dividing the input dataset $x = (e(t), \frac{de(t)}{dt})$ (Table 1) into k predetermined clusters [66]. Each cluster groups objects that are more similar to each other than to objects in different clusters [67]. This process continues until minimal change occurs in the centroids or the iteration's specified number is completed [68–71]. Cluster analysis of the training data (Table 1) revealed eight clusters (I...VIII). The training and test sets were formed in a 2:1 ratio (67 and 33%, respectively) based on random selection. Both datasets showed the presence of eight clusters, indicating a similar composition. The distances between clusters were nearly identical across both sets, confirming their similarity (Figure 7).
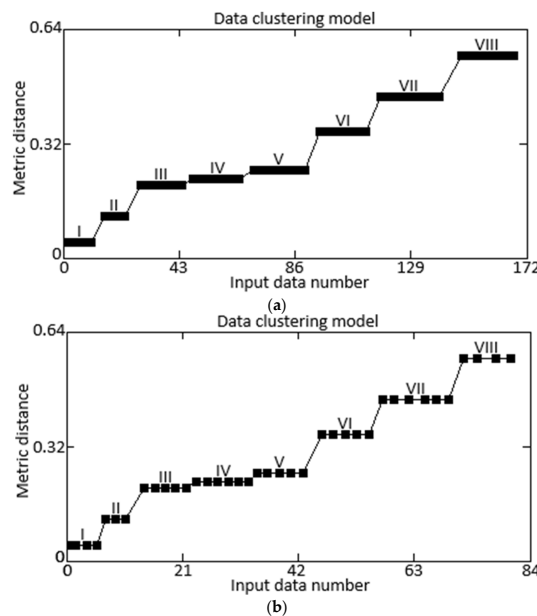

Figure 7. Cluster analysis results: (**a**) training dataset; (**b**) test dataset.

Consequently, the optimal sample sizes were established as follows: the training dataset contains 256 elements (100%), the control dataset has 172 elements (67% of the training dataset), and the test dataset includes 84 elements (33% of the training dataset).

3.2. Results of Computational Experiment

A semi-physical modeling stand (SPMS) was developed to conduct the computational experiment, representing an improved version of a similar stand previously designed [57]. This SPMS is intended to simulate helicopter TE parameters in real time and replicate operational modes within altitude and flight speed ranges. Additionally, it facilitates interaction with higher-level systems through data exchange channels, testing the control system unit and addressing other tasks [57]. Figure 8 illustrates the interaction scheme between the developed neuro-fuzzy network (Figure 5) and the SPMS. On the SPMS, the helicopter TE malfunctions are displayed by introducing artificial perturbations into the model parameters or modifying the input data corresponding to certain failure scenarios. The neural network model integrated into the stand analyzes changes in the dynamics of parameters such as rotor speed, temperature indicators, and fuel consumption, which allows us to identify deviations associated with malfunctions. This provides an opportunity to test the developed control system's stability and assess its adaptability in the event of failures.
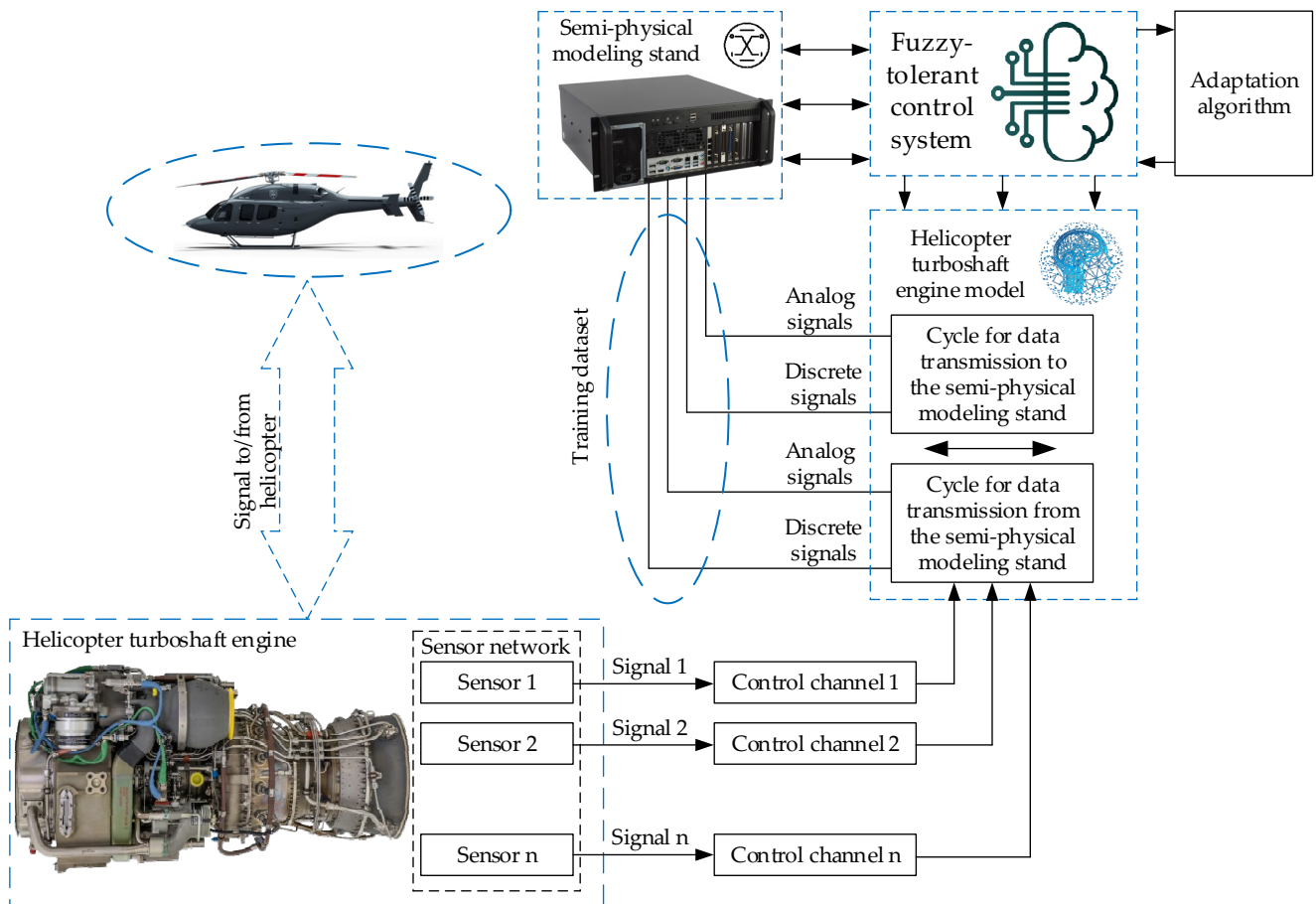
Figure 8. A scheme showing the interaction between the helicopter turboshaft engine model and the semi-physical simulation stand.

The research examines an example of constructing a failure model related to the fuel flow actuator G_T control loss, which is the gas generator rotor r.p.m. n_{TC} channel. The failure model, represented as a production rule set (the fuel flow actuator $H = 0$, $M = 0$ failure), is expressed as follows:

$$\text{Rule 1}: \text{If } e_{n_{TC}} > 0.706 \text{ and } \frac{\partial e_{n_{TC}}(t)}{\partial t} \leq -0.00027, \text{ then } u_{n_{TC}} = 4.383 - 6.708 \cdot e_{n_{TC}} - 0.336 \cdot \frac{\partial e_{n_{TC}}(t)}{\partial t},$$
$$\text{Rule 2}: \text{If } e_{n_{TC}} > 0.707 \text{ and } e_{n_{TC}} \leq -0.00028, \text{ then } u_{n_{TC}} = -1.113 + 1.003 \cdot e_{n_{TC}},$$
$$\text{Rule 3}: \text{If } e_{n_{TC}} > 0.709, \text{ then } u_{n_{TC}} = -1.136 + 1.013 \cdot e_{n_{TC}}, \tag{43}$$
$$\text{Rule 4}: \text{If } e_{n_{TC}} \leq 0.706 \text{ and } \frac{\partial e_{n_{TC}}(t)}{\partial t} \leq -0.00027, \text{ then } u_{n_{TC}} = -5.993 + 8.029 \cdot e_{n_{TC}} + 0.487 \cdot \frac{\partial e_{n_{TC}}(t)}{\partial t},$$
$$\text{Rule 5}: \text{If } e_{n_{TC}} \leq 0.71 \text{ and } \frac{\partial e_{n_{TC}}(t)}{\partial t} \leq -0.00027, \text{ then } u_{n_{TC}} = -0.011 + 0.492 \cdot e_{n_{TC}} + 0.117 \cdot \frac{\partial e_{n_{TC}}(t)}{\partial t}.$$

Figure 9 presents the failure $u_{n_{TC}} = f\left(e_{n_{TC}}, \frac{\partial e_{n_{TC}}(t)}{\partial t}\right)$ "profile", where $e_{n_{TC}}$ is the signal representing the change in the control error in the rotational speed channel; $\frac{\partial e_{n_{TC}}(t)}{\partial t}$ represents the error signal derivative.
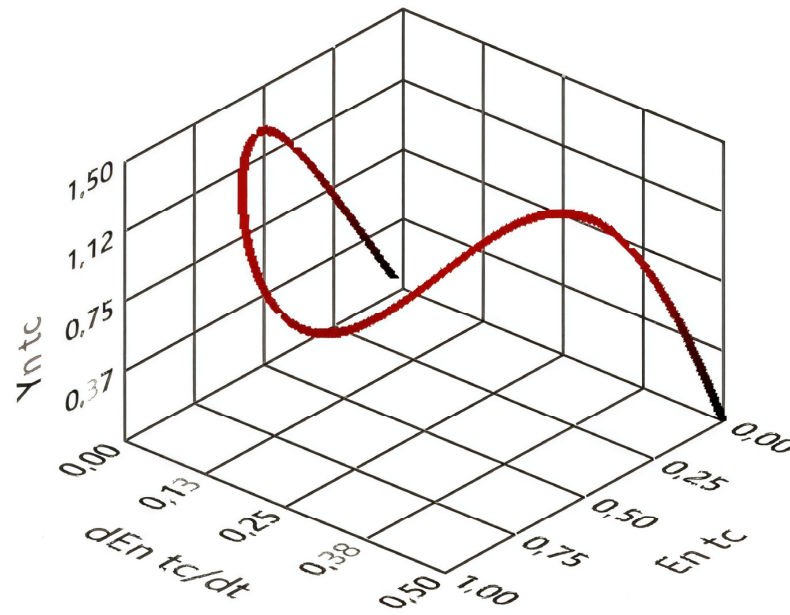

Figure 9. Failure "profile" diagram related to fuel flow actuator control loss.

The developed failure models are stored in the control system's knowledge base and are utilized to assess the control situation to generate corrective actions to switch control channels for helicopter gas turbine engines. The study investigates the transient characteristics of the failure model related to the control loss in the fuel flow actuator within the gas generator rotor r.p.m. channel (Figure 10).
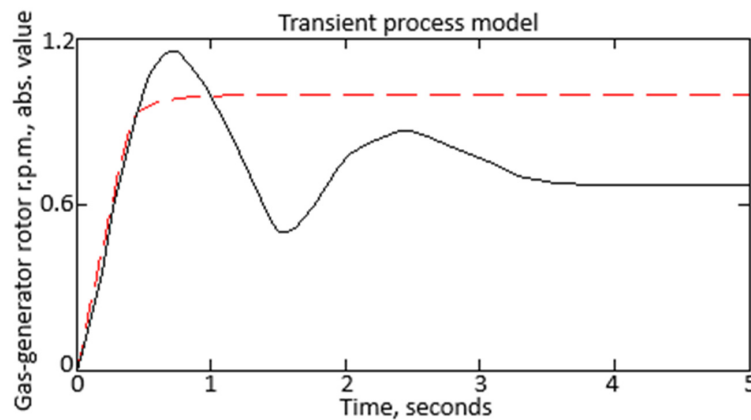

Figure 10. The diagram of the transient process during the fuel flow actuator control loss is the gas-generator rotor r.p.m. channel.

In Figure 10, surge and decay indicate the sudden failure of the fuel flow actuator. This failure resulted in a sharp reduction in fuel supply, leading to a drop in gas generator rotor r.p.m. and a deterioration in engine dynamics. The dotted red line on the diagram represents the engine's trajectory under normal operating conditions for comparison with the failure scenario.

The fault tolerance degree for the helicopter TE FTCS (Figure 4) was assessed by determining the limiting value of the cost function over the investigated time interval (from 0 to 320 s) (Figure 11). The allowable threshold value for the cost function was set at 1, based on the normalization of all parameters. According to the diagram, the cost function limiting value within the time interval from 0 to 320 s is 0.137. This indicates that the developed helicopter TE FTCS demonstrates high fault tolerance, as the cost function value is significantly below the established permissible level. A value of 0.137 indicates that the system successfully controls deviations from target values while minimizing control efforts and the impact of external disturbances within the specified time interval.
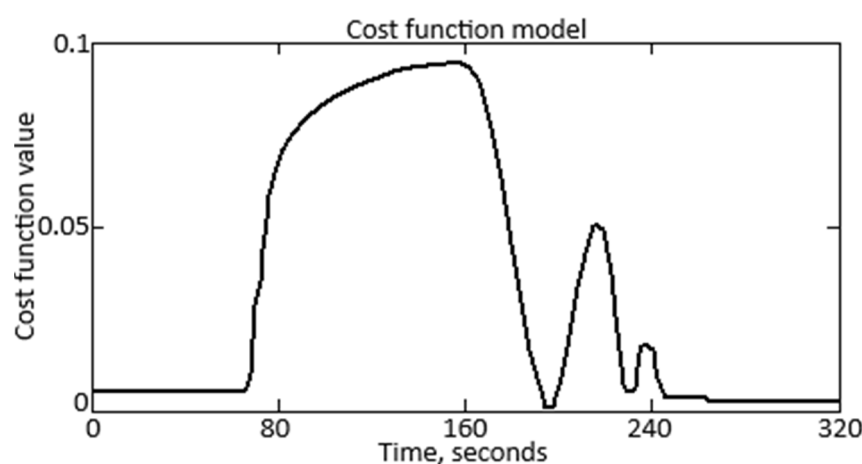
Figure 11. A diagram of the cost function change during the researched interval from 0 to 320 s.

A system stable state is achieved when the cost function value $J < 0.5$, which indicates a high degree of fault tolerance and the system's ability to effectively control deviations from target values. In a neutral state, with $J \approx 0.5$ to $J < 1$, the system begins to exhibit tendencies toward unstable oscillations, requiring increased sensitivity in control actions and the implementation of adaptive algorithms to maintain control. In the case of an unstable state, when $J \geq 1$, the system demonstrates unpredictable behavior and damage risks, necessitating a sharp reduction in control actions and the use of the developed helicopter TE FTCS (Figure 3) application to eliminate deviations and ensure safe operation.

3.3. Neural Network Model Quality Evaluation

Since the basis for the developed helicopter TE FTCS (Figure 4) is a neuro-fuzzy network (Figure 3), evaluating neuro-fuzzy network quality is reasonable. It allows for the determination of how effectively the neuro-fuzzy network addresses control tasks and makes decisions under uncertainty and variability. The evaluation includes analyzing its generalization ability, prediction accuracy, and resilience to external disturbances. Performance assessment for the developed neuro-fuzzy network (Figure 5) uses vital quality metrics such as accuracy, loss, precision, recall, F1-metric, and AUC-ROC [72–78]. These metrics comprehensively evaluate the neuro-fuzzy network's effectiveness in various aspects of its operation within the controlling helicopter TE context. Accuracy helps identify the proportion of correctly classified engine operating modes relative to the total number, providing insights into the model's overall performance. Loss measures how well the model aligns with actual data, indicating the need for further optimization in control strategies. Precision and recall offer insights into the accuracy and completeness of identifying critical engine states, which is especially important for preventing malfunctions. The F1-metric,

representing the harmonic mean of Precision and Recall, helps balance these two indicators, which are critical in resource-limited conditions and high safety requirements. AUC-ROC provides information on the model's ability to distinguish between normal and emergency engine states at various thresholds, which is essential for assessing the reliability of the control system. This comprehensive metrics analysis allows for the neuro-fuzzy network's current performance evaluation and identifies areas for improvement, ultimately enhancing the developed helicopter TE FTCS's efficiency. These metrics are calculated according to the following expressions [73,75,77,79,80]:

$$
\begin{gathered}
Accuracy = \frac{1}{N} \cdot \sum_{i=1}^{N} \mathbf{1}(u_i = \hat{u}_i), \ Loss = \frac{1}{N} \cdot \sum_{i=1}^{N} (u_i(t) - \hat{u}_i(t))^2, \\
Precision = \frac{TP}{TP+FP}, \ Recall = \frac{TP}{TP+FN}, \ F1-score = \frac{2 \cdot Precision \cdot Recall}{Precision + Recall}, \\
AUC - ROC = \int_0^1 TPR \cdot \left(FPR^{-1}(t)\right) dt.
\end{gathered}
\tag{44}
$$

In this scenario, u_i denotes the actual label for the *i*-th instance, whereas $\hat{u}_i$ signifies the predicted label generated by the model for that particular instance. *N* represents the total number of examples in the dataset (applicable for either training or validation), and the indicator function $\mathbf{1}(u_i = \hat{u}_i)$ yields a value of 1 if the true and predicted labels match and 0 otherwise. In the helicopter TE control context, the metrics *TP* (True Positive), *TN* (True Negative), *FP* (False Positive), *FN* (False Negative), *TPR* (True Positive Rate), and *FPR* (False Positive Rate) play a key role in assessing the monitoring and diagnostic systems' effectiveness [51,57,81]. *TP* represents instances when the system successfully detects faults, while *TN* indicates incorrect identification. *FP* refers to erroneous signals about faults, and *FN* describes missed critical conditions. $TPR = \frac{TP}{TP+FN}$, or sensitivity, reflects the proportion of correctly identified faults among all actual cases, which is vital for enhancing safety, while $FPR = \frac{FP}{FP+TN}$ represents the level of false alarms [82–86]. Analyzing these metrics allows for an evaluation of system reliability, identifying shortcomings in diagnostic algorithms and implementing necessary adjustments to improve flight safety.

Figures 12 and 13 illustrate the diagrams for accuracy and loss metrics. The accuracy metric for the developed neuro-fuzzy network (Figure 5) achieves 99.455% following 250 training epochs while addressing the helicopter TE control challenge. This remarkable performance highlights the model's capability to manage the helicopter TE control task across different conditions.

Additionally, the loss associated with the neuro-fuzzy network (Figure 5) declines from 2.5 to 0.5% after 250 training epochs in tackling the helicopter TE control task. Such improvements in accuracy and loss indicate a well-optimized model, reinforcing its potential for reliable application in real-world scenarios. The findings suggest that further refinements may enhance the network's adaptability and performance in dynamic operating environments.
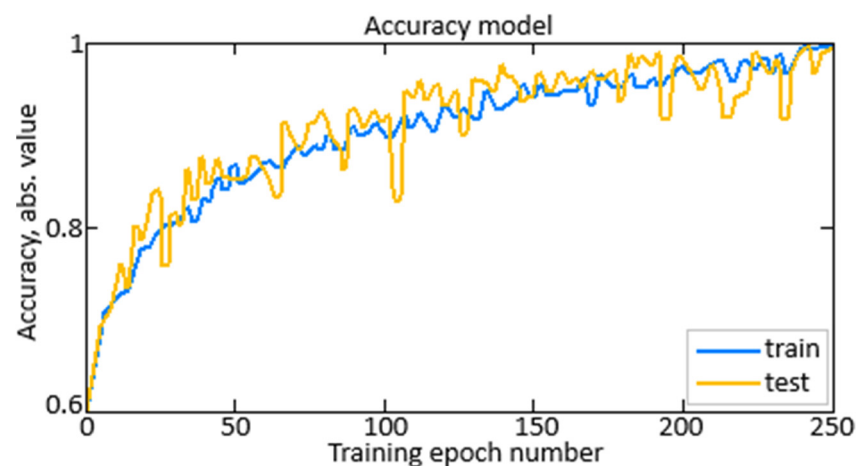

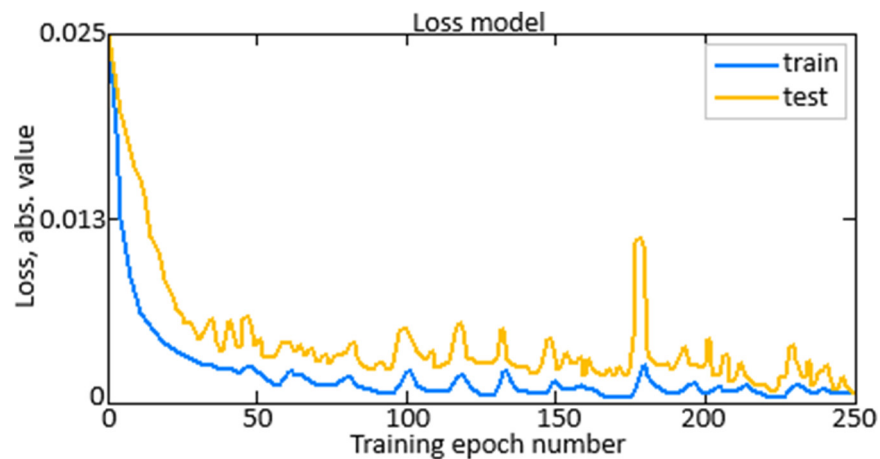**Figure 12.** Accuracy metric diagram.

Figure 13. Loss metric diagram.

The created neuro-fuzzy network attains a precision score of 0.981, a recall score of 1.0, and an F1-score of 0.990 in the helicopter TE control task under various conditions. These metrics reflect exceptional accuracy and dependability in detecting faults while ensuring zero false negatives. The F1-score also illustrates the model's balanced effectiveness concerning precision and recall. The results obtained were compared (Tables 3 and 4) with four other approaches: 1 is the neural network-based closed three-channel onboard helicopter TE ACS, 2 is the neuro-fuzzy onboard helicopter TE ACS based on ANFIS architecture, 3 is the neuro-fuzzy onboard helicopter TE ACS based on AFNN architecture, and 4 is the traditional helicopter TE ACS.

Table 3. Comparative analysis results.

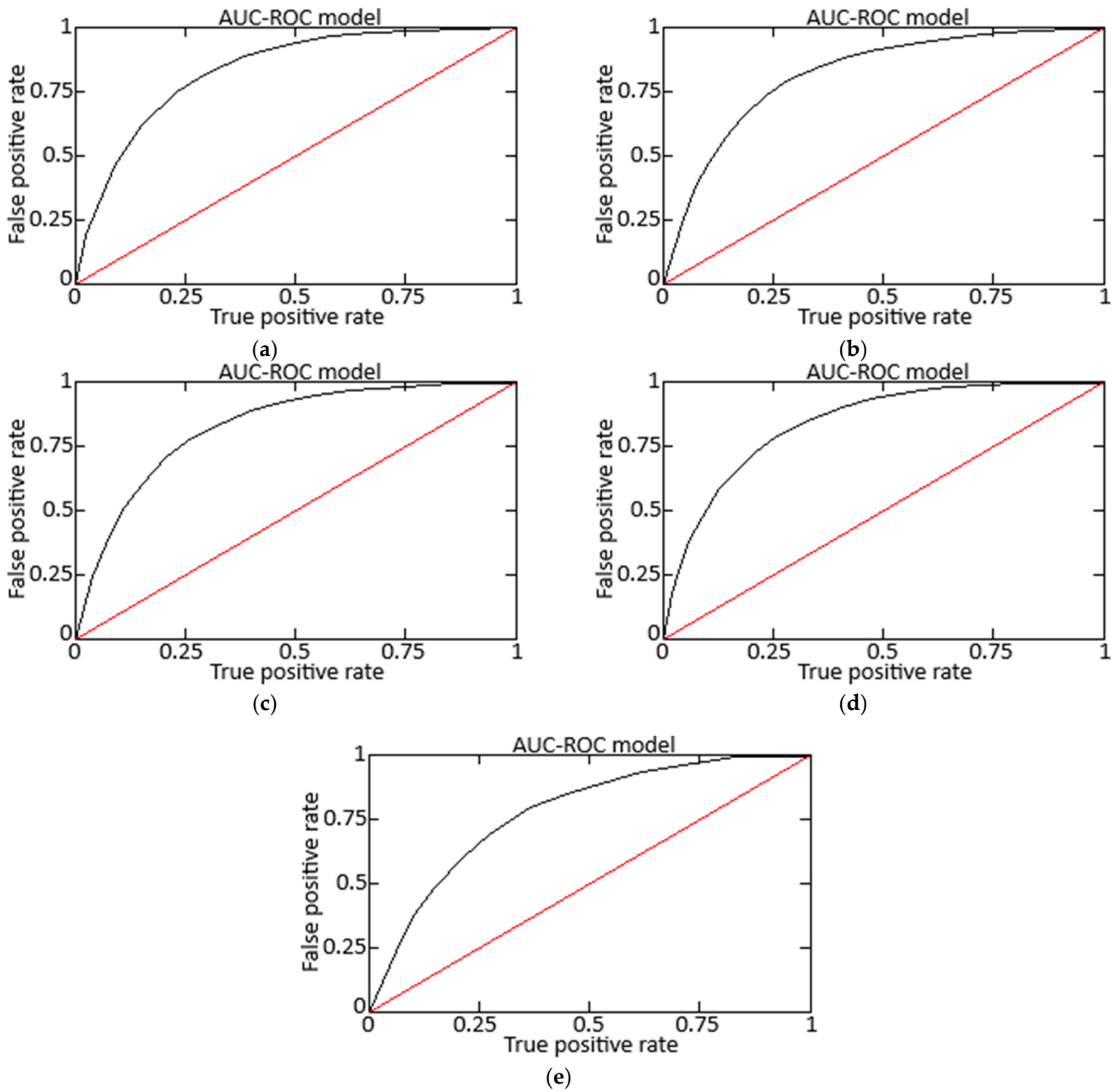| Metric	Proposed Approach	Alternative Approach 1	Alternative Approach 2	Alternative Approach 3	Alternative Approach 4
Accuracy	0.995 (99.5%)	0.961 (96.1%)	0.975 (97.5%)	0.999 (99.9%)	0.882 (88.2%)
Precision	0.981 (98.1%)	0.953 (95.3%)	0.962 (96.2%)	0.986 (98.6%)	0.869 (86.9%)
Recall	1.0	0.983	0.988	1.0	0.909
F1-score	0.990	0.973	0.975	0.993	0.889

Table 4. Comparative analysis results (AUC-ROC analysis).

Metric	Proposed Approach	Alternative Approach 1	Alternative Approach 2	Alternative Approach 3	Alternative Approach 4
True Positives	96	90	92	99	85
True Negatives	4	10	8	1	15
False Positives	287	282	284	291	277
False Negatives	14	20	18	11	25
True Positive Rate	0.828	0.785	0.793	0.844	0.626
False Positive Rate	0.0101	0.0169	0.0152	0.0097	0.0235
False Negative Rate	0.0098	0.0109	0.0103	0.0093	0.0192
AUC-ROC	0.831	0.773	0.791	0.848	0.651

The comparative analysis of various approaches to helicopter TE control reveals that the proposed method demonstrates a high accuracy (99.5%) and F1-score (0.990), confirming its effectiveness and reliability. In contrast, alternative methods show varying results, with Approach 4 having a significantly lower accuracy value of 88.2%. Approaches 1 and 2 exhibit satisfactory outcomes but fall short compared to the proposed solution. Notably, the proposed method achieves a perfect recall value of 1.0, indicating complete identification

of all positive cases. These results highlight significant advantages in the proposed FTCS for helicopter TE control compared to other examined methods.

The comparative analysis (Table 4 and Figure 14) highlights significant performance differences among various approaches to helicopter TE control. The proposed method excels with the highest True Positive Rate (0.828) and True Positives (96), indicating superior fault detection capabilities. In contrast, Alternative Approaches 1 and 2 show lower True Positive Rates (0.785 and 0.793, respectively). The proposed method also maintains a low False Positive Rate (0.0101) compared to Alternatives 1 (0.0169) and 4 (0.0235) while achieving an AUC-ROC score of 0.831, surpassing the other approaches. The proposed approach demonstrates effective fault detection with minimal false alarms, establishing its efficacy in helicopter TE control tasks.

Figure 14. The AUC-ROC diagrams: (**a**) the proposed approach; (**b**) the Alternative Approach 1; (**c**) the Alternative Approach 2; (**d**) the Alternative Approach 3; (**e**) the Alternative Approach 4.

The proposed approach significantly increases the helicopter's operational efficiency and safety due to more accurate control and effective malfunction detection. In comparison with traditional control systems (Approach 4), which demonstrate significantly lower accuracy (88.2%) and a higher frequency of false alarms (0.0235), the proposed system provides high accuracy (99.5%) with a minimal frequency of false alarms (0.0101). This helps to reduce the in-flight failure probability and allows for timely detection of potential malfunctions, which is critically important for increasing operational reliability. In addition, high completeness (recall 1.0) allows you to minimize the risk of missing critical situations, which improves the overall perception of pilot safety.

4. Discussion

This study focuses on developing an innovative helicopter TE FTCS (see Figure 4). The proposed helicopter TE FTCS (see Figure 4) includes a fuzzy regulator, an adaptation and reconfiguration unit, a control channel selector, an actuator block, a helicopter TE model, a fuel metering needle model, and a sensor block. The fuzzy regulator consists of a fuzzifier, inference mechanism, defuzzifier, fuzzy rule base, and monitoring block. The key distinction lies in separating the helicopter TE and FMU models, improving control accuracy and adaptability to changing conditions. To achieve this, the helicopter TE operation innovative control law (23) has been proposed, differing from the traditional approach by using an adaptive control system instead of static settings. This system dynamically adjusts fuel supply and the blade pitch angle. The model is based on maintaining free turbine rotor speed, which is crucial for safe piloting while accounting for changing flight conditions such as altitude, temperature, and power.

The helicopter TE chosen for the computational experiment was the TV3-117, installed on an Mi-8MTV helicopter. Engine parameters (n_{TC}, n_{FT}, T_G^*, etc.) were collected exclusively from flight data recorded during helicopter trials. The data were logged using D-2M and D-1M sensors and 14 pairs of T-101 thermocouples over 320 s of actual flight time at a frequency of one per second (see Figure 1). A simulation test stand (see Figure 8) was developed, representing an improved version of the stand described earlier in [57]. The test stand simulates helicopter TE parameters in real time and reproduces operating modes across a range of altitudes and airspeeds. Moreover, it supports interactions with higher-level systems through data exchange channels, allowing for control unit testing and performing other tasks [57].

The research explored failure modeling related to the control loss in the fuel supply actuator within the gas generator rotor r.p.m. channel. A failure model (see Figure 9) was created as a production rule comprising conditions and actions describing system behavior during failure scenarios. This model accounts for dynamic changes in system parameters and probabilistic failure characteristics, enabling the prediction of potential malfunctions and their impact on gas generator operation. Production rules (43) are used for the failure scenarios' automatic generation and their effects on subsequent system performance analysis, which is essential for developing reliable diagnostic and control methods in natural operational environments.

The failure model transient characteristic analysis, associated with control loss in the fuel supply actuator within the turbo-compressor rotor speed channel, showed that sudden failure (surge and decay in Figure 10) causes a sharp drop in fuel supply. This results in reduced rotor speed and impaired engine dynamics. For comparison, the standard engine trajectory is shown as a dashed red line in Figure 10, highlighting the failure's impact on system performance.

The developed helicopter TE FTCS fault tolerance assessment (see Figure 11) revealed that the cost function's maximum value during the studied time interval (from 0 to 320 s) is 0.137, significantly below the allowable value of 1, which is set for normalized parameters. This indicates a high degree of fault tolerance in the system, effectively controlling deviations from target values while minimizing control efforts and the effects of external disturbances during the specified period.

The neuro-fuzzy network's (see Figure 5) quality, forming the developed helicopter TE FTCS's (see Figure 4) foundation, was evaluated using traditional metrics such as accuracy, loss, precision, recall, F1-score, and AUC-ROC. Figures 12 and 13 present accuracy and loss diagrams. The developed neuro-fuzzy network's (Figure 5) accuracy reaches 99.455% after 250 training epochs in the helicopter engine control task, demonstrating the model's high efficiency under various conditions. The loss function decreases from 2.5 to 0.5% over the same training period. These results suggest good model optimization and reliability for practical applications, with the potential for further improvements in adaptability and performance under dynamic operational conditions.

The helicopter TE control task comparative analysis (see Tables 3 and 4) using the developed neuro-fuzzy control system (see Figure 4) was conducted against four alternative approaches: 1 is the neural closed-loop triple-channel onboard control system, 2 is the neuro-fuzzy onboard system based on ANFIS, 3 is the neuro-fuzzy onboard system based on AFNN, and 4 is the traditional control system. The comparative analysis revealed that the proposed method demonstrates a high accuracy (99.5%) and F1-score (0.990), confirming its effectiveness and reliability. In contrast, the alternative approaches showed less satisfactory results, particularly Approach 4, with an accuracy of 88.2%. Approaches 1 and 2 provided acceptable results but were outperformed by the proposed solution, which also features perfect recall (recall is 1.0), indicating the full recognition of all present positive cases. As shown in Table 4 and Figure 14, the proposed method surpasses the others in terms of fault detection, with the highest true positive rate (0.828) and the lowest false alarm rate (0.0101), supported by an AUC-ROC of 0.831.

Thus, the developed FTCS (see Figure 4) application on board helicopters improves control efficiency and reduces accident probability [87–92], providing better integration of expert knowledge and enhancing resilience to uncertainties and external factors.

However, this study's one limitation is the exclusive use of flight data from a specific engine type (TV3-117), which may restrict the results' generalizability to other engine types or operating conditions. Additionally, the proposed control model requires precise tuning and calibration of system parameters for different flight modes, which may complicate its implementation on real helicopters, especially for significant changes faced in operating conditions or system configuration. Furthermore, variations in flight conditions, such as altitude, temperature, or load fluctuations, may lead to discrepancies in the model's performance if not accounted for during the calibration process. The model's reliance on specific engine characteristics also limits its adaptability, potentially requiring significant reconfiguration or retraining when applied to engines with differing dynamic behaviors or performance parameters.

Future research directions include extending the model to other engine types [93–96] and aircrafts [97,98] and integrating more advanced machine learning [99,100] and predictive methods, such as deep neural networks [101,102] and reinforcement learning techniques [103–105], to enhance the system's adaptability to dynamic flight conditions. Furthermore, optimizing computational costs and developing self-correction algorithms [106,107] could improve system reliability and fault tolerance in real time. In future directions of research, models will be developed in which clear systems and machine learning methods will be integrated in the current model to improve context. Mentioning specific approaches would provide more effective guidance and better support the future relevance of the research. In addition, future directions of research will include the development of a potential extension of the model to engines and aircrafts of other types [108–111]. Also, discussing the possible problems of more advanced machine learning methods and how they could contribute to the system's adaptability will provide more context and justify the proposed future directions. It is also planned to calculate the added value for demonstration in experimental research.

5. Conclusions

This study focuses on the development of a helicopter turboshaft engine innovative fault-tolerant fuzzy automatic control system, significantly enhancing management efficiency in various flight modes. The research presents an innovative structure of a fuzzy control system, including a fuzzy controller, adaptation and reconfiguration modules, and a control channel selector. The key achievement is the helicopter turboshaft engines model's separation and the fuel metering unit; the system's responsiveness to changing conditions increases while achieving a control accuracy of more than 99%. The conducted computational experiment is focused on the TV3-117 turboshaft engine installed on the Mi-8MTV helicopter, with engine data collected using high-precision sensors during flight tests (D2-M, D-1M, etc.). A special test stand was developed to reproduce working conditions, which allowed us to evaluate the system's dynamics and detect potential malfunctions.

The results showed a high degree of fault tolerance for the developed system, with a cost function limit significantly below the acceptable level. The quality of the neuro-fuzzy network as the foundation for the automatic control system confirmed its effectiveness, achieving an accuracy of 99.455%. A comparative analysis with alternative approaches indicated that the proposed methodology significantly outperforms traditional solutions, providing higher fault recognition and minimizing false alarms.

Despite the fact that notable successes were achieved, the research is limited by relying on data from flight tests of one type of engine, which potentially limits the wider applicability of its results. Moreover, the system's requirement for careful adjustment of control parameters in various flight modes creates problems for practical deployment. Prospects for further research are focused on expanding the model to cover a wider range of engines and aircrafts with the inclusion of advanced machine learning methods [108–111]. The proposed fault-tolerant fuzzy control system demonstrates significant prospects for controlling an aircraft's flight, in particular, helicopters [87,88]. By combining expert knowledge with adaptive control strategies, the developed fault-tolerant fuzzy control system effectively eliminates uncertainties and external failures (achieved accuracy of more than 99%), positioning itself as a valuable tool for use in civil and military aviation.

Nomenclature

G_T	is the fuel supply;
$\varphi_{m.r.}$	is the central rotor blade pitch angle;
n_{FT}	is the free turbine rotor speed;
n_{TC}	is the gas generator rotor r.p.m.;
T_G^*	is the gas temperature in the front of the compressor turbine;
N_e	is the engine output shaft power;

H	is the flight altitude;
P_α	is the ambient air pressure;
T_α	is the ambient air temperature;
η_{FT}	is the free turbine efficiency;
$\dot{Q}$	is the fuel combustion thermal power;
N_{FT}	is the free turbine power;
$N_{m.r.}$	is the main rotor power;
$N_{power\ loss}$	is the power loss (for transmission and resistance);
H_u	is the fuel combustion heat;
c_p	is the gas specific heat capacity
$C_T(\varphi_{m.r.})$	is the thrust coefficient depending on the blade angle;
ρ	is the air density;
$A_{m.r.}$	is the main rotor area;
$T_{m.r.}$	is the required main rotor thrust;
k_H	is the coefficient of change in fuel supply with altitude;
H_{max}	is the maximum design altitude;
k_T	is the coefficient of dependence of fuel supply on ambient temperature;
T_N	is the nominal temperature;
G_T^{lim}	is the limited fuel supply consistent with safe operating conditions;
G_T^{base}	is the base fuel supply;
α and β	are the adaptation coefficients for power and rotation speed, respectively;
J_{FT}	is the free turbine inertia moment;
$M_{FT}(t)$	is the torque from the free turbine;
$M_{m.r.}(t)$	is the main rotor resistance moment;
k_G and k_φ	are the gain factors for regulating fuel supply and blade angle;
$\tilde{x}$	are the fuzzy values;
$\mu_A(x)$	is the membership function;
y	is the output value;
θ	are the control parameters;
c_i	is the membership function center;
σ_i	is the membership function width;
γ	is the adaptation rate;
$y_{desired}$ and y_{actual}	are the desired and actual output values;
μ	is a factor defining the adaptation degree;
δ	is the control parameter;
ω	is the disturbance and noise;
D	is the fuel metering unit position;
k	is the gain coefficient;
c	is the damping coefficient;
u	is the control action;
e	is the control error
K_p, K_i, and K_d	are the proportional, integral, and derivative gains, respectively;
S	is the measured value;
h	is the measurement function;
ϵ	is the measurement error;
$u_0(t)$	is the control signal under normal operating conditions;
$u_c(t)$	is the corrective action dependent on the failure vector;
$d(t)$	is the failure vector;
$x_{ref}(t)$	are the target system parameters;
γ_1 and γ_2	are weights defining the contribution of control actions and failures to the total cost;
γ	is the iteration step size.

References

1. Song, J.; Wang, Y.; Ji, C.; Zhang, H. Real-Time Optimization Control of Variable Rotor Speed Based on Helicopter/Turboshaft Engine Onboard Composite System. *Energy* **2024**, *301*, 131701. [CrossRef]
2. Wang, Y.; Ji, C.; Xi, Z.; Zhang, H.; Zhao, Q. An Adaptive Matching Control Method of Multiple Turboshaft Engines. *Eng. Appl. Artif. Intell.* **2023**, *123*, 106496. [CrossRef]
3. Yepifanov, S.; Bondarenko, O. Forming of turboshaft engine mathematical model. *Aerosp. Tech. Technol.* **2023**, *4*, 85–94. [CrossRef]

4. Donateo, T.; Cucciniello, L.; Strafella, L.; Ficarella, A. Control Oriented Modelling of a Turboshaft Engine for Hybrid Electric Urban Air-Mobility. *E3S Web Conf.* **2020**, *197*, 05003. [CrossRef]

5. Wang, Y.; Zheng, Q.; Xu, Z.; Zhang, H. A Novel Control Method for Turboshaft Engine with Variable Rotor Speed Based on the Ngdot Estimator Through LQG/LTR and Rotor Predicted Torque Feedforward. *Chin. J. Aeronaut.* **2020**, *33*, 1867–1876. [CrossRef]

6. He, D.; Zhang, R.; Wen, C.; Chen, L. A Control Framework for Turboshaft Engine Based on Thermo-Gas-Dynamic Model. In Proceedings of the Eighth International Conference on Electromechanical Control Technology and Transportation (ICECTT 2023), Hangzhou, China, 19–21 May 2023; Volume 12790. [CrossRef]

7. Ahmadian, N.; Khosravi, A.; Sarhadi, P. Adaptive Control of a Jet Turboshaft Engine Driving a Variable Pitch Propeller Using Multiple Models. *Mech. Syst. Signal Process.* **2017**, *92*, 1–12. [CrossRef]

8. Sheng, H.; Zhang, T.; Jiang, W. Full-Range Mathematical Modeling of Turboshaft Engine in Aerospace. *Int. J. Turbo Jet Engines* **2015**, *33*, 309–317. [CrossRef]

9. Yepifanov, S.; Bondarenko, O. Development of Turboshaft Engine Adaptive Dynamic Model: Analysis of Estimation Errors. *Trans. Aerosp. Res.* **2022**, *4*, 59–71. [CrossRef]

10. Zou, W.; Song, Z.; Wang, B.; Wen, M.; Zheng, X. An Efficient Multi-Fidelity Simulation Approach for Performance Prediction of Adaptive Cycle Engines. *J. Glob. Power Propuls. Soc.* **2024**, *8*, 310–322. [CrossRef]

11. Lan, J.; Patton, R.J.; Punta, E. Fault-Tolerant Tracking Control for A 3-DOF Helicopter with Actuator Faults and Saturation. *IFAC-PapersOnLine* **2017**, *50*, 5250–5255. [CrossRef]

12. Wang, Y.; Zheng, Q.; Du, Z.; Zhang, H. Research on Nonlinear Model Predictive Control for Turboshaft Engines Based on Double Engines Torques Matching. *Chin. J. Aeronaut.* **2020**, *33*, 561–571. [CrossRef]

13. Wang, H.; Wang, D.; Zhang, G. *Research of Neural Network PID Control of Aero-Engine*; Lecture Notes in Electrical Engineering; Springer: Berlin/Heidelberg, Germany, 2011; Volume 122, pp. 337–343. [CrossRef]

14. Castiglione, T.; Perrone, D.; Strafella, L.; Ficarella, A.; Bova, S. Linear Model of a Turboshaft Aero-Engine Including Components Degradation for Control-Oriented Applications. *Energies* **2023**, *16*, 2634. [CrossRef]

15. Gu, N.; Wang, X. Model Predictive Controller Design Based on the Linear Parameter Varying Model Method for a Class of Turboshaft Engines. In Proceedings of the 2018 Joint Propulsion Conference, Cincinnati, OH, USA, 9–11 July 2018. [CrossRef]

16. Lu, F.; Huang, J.; Xing, Y. Fault Diagnostics for Turbo-Shaft Engine Sensors Based on a Simplified Onboard Model. *Sensors* **2012**, *12*, 11061–11076. [CrossRef]

17. Wu, W.-C.; Meen, T.-H. Use of Sensor Data of Aircraft Turbine Engine for Education of Aircraft Maintenance. *Sens. Mater.* **2023**, *35*, 733. [CrossRef]

18. Ranjbar, A.; Khosravi, A.; Ahmadian, N. Control of a Jet Engine Using Predictor-Based Adaptive Strategy in Different Flight Modes. *J. Syst. Control. Eng.* **2023**, *237*, 1349–1364. [CrossRef]

19. Sheng, H.; Chen, Q.; Li, J.; Jiang, W.; Wang, Z.; Liu, Z.; Zhang, T.; Liu, Y. Research on Dynamic Modeling and Performance Analysis of Helicopter Turboshaft Engine's Start-Up Process. *Aerosp. Sci. Technol.* **2020**, *106*, 106097. [CrossRef]

20. Cheng, K.; Wang, Y.; Yang, X.; Zhang, K.; Liu, F. An Intelligent Online Fault Diagnosis System for Gas Turbine Sensors Based on Unsupervised Learning Method LOF and KELM. *Sens. Actuators A Phys.* **2024**, *365*, 114872. [CrossRef]

21. Pérez-Ventura, U.; Fridman, L.; Capello, E.; Punta, E. Fault Tolerant Control Based on Continuous Twisting Algorithms of a 3-DoF Helicopter Prototype. *Control Eng. Pract.* **2020**, *101*, 104486. [CrossRef]

22. Bovsunovsky, A.; Nosal, O. Highly Sensitive Methods for Vibration Diagnostics of Fatigue Damage in Structural Elements of Aircraft Gas Turbine Engines. *Procedia Struct. Integr.* **2022**, *35*, 74–81. [CrossRef]

23. Boujamza, A.; Lissane Elhaq, S. Attention-Based LSTM for Remaining Useful Life Estimation of Aircraft Engines. *IFAC-PapersOnLine* **2022**, *55*, 450–455. [CrossRef]

24. Kumar, S.R.; Devakumar, J. Recurrent Neural Network Based Sensor Fault Detection and Isolation for Nonlinear Systems: Application in PWR. *Prog. Nucl. Energy* **2023**, *163*, 104836. [CrossRef]

25. Szrama, S.; Lodygowski, T. Aircraft Engine Remaining Useful Life Prediction Using Neural Networks and Real-Life Engine Operational Data. *Adv. Eng. Softw.* **2024**, *192*, 103645. [CrossRef]

26. Balli, O. Exergetic, sustainability and environmental assessments of a turboshaft engine used on helicopter. *Energy* **2023**, *276*, 127593. [CrossRef]

27. Zheng, X.; Zeng, H.; Wang, B.; Wen, M.; Yang, H.; Sun, Z. Numerical simulation method of surge experiments on gas turbine engines. *Chin. J. Aeronaut.* **2023**, *36*, 107–120. [CrossRef]

28. Lyu, K.; Tan, X.; Liu, G.; Zhao, C. Sensor Selection of Helicopter Transmission Systems Based on Physical Model and Sensitivity Analysis. *Chin. J. Aeronaut.* **2014**, *27*, 643–654. [CrossRef]

29. Aygun, H.; Turan, O. Exergetic sustainability off-design analysis of variable-cycle aero-engine in various bypass modes. *Energy* **2020**, *195*, 117008. [CrossRef]

30. Zhao, Y.-P.; Huang, G.; Hu, Q.-K.; Li, B. An improved weighted one class support vector machine for turboshaft engine fault detection. *Eng. Appl. Artif. Intell.* **2020**, *94*, 103796. [CrossRef]

31. Wang, B.; Wang, F.; Zhang, X.; Wang, J.; Xue, T. Numerical analysis of cooling efficiency for turboshaft engines with converging-diverging film cooling holes. *Int. J. Therm. Sci.* **2023**, *185*, 108044. [CrossRef]

32. Jiang, P.; Xiong, S.; Xu, W.; Du, Z.; He, X. Experimental study on the combustion performance of a turboshaft engine annular combustor. *J. Energy Inst.* **2023**, *111*, 101412. [CrossRef]

33. Han, D.; Pastrikakis, V.; Barakos, G.N. Helicopter performance improvement by variable rotor speed and variable blade twist. *Aerosp. Sci. Technol.* **2016**, *54*, 164–173. [CrossRef]

34. Abdalla, M.S.M.; Balli, O.; Adali, O.H.; Korba, P.; Kale, U. Thermodynamic, sustainability, environmental and damage cost analyses of jet fuel starter gas turbine engine. *Energy* **2023**, *267*, 126487. [CrossRef]

35. Vladov, S.; Banasik, A.; Sachenko, A.; Kempa, W.M.; Sokurenko, V.; Muzychuk, O.; Pikiewicz, P.; Molga, A.; Vysotska, V. Intelligent Method of Identifying the Nonlinear Dynamic Model for Helicopter Turboshaft Engines. *Sensors* **2024**, *24*, 6488. [CrossRef] [PubMed]

36. Han, X.; Huang, J.; Zhou, X.; Zou, Z.; Lu, F.; Zhou, W. A Novel, Reduced-Order Optimization Method for Nonlinear Model Correction of Turboshaft Engines. *J. Mech. Sci. Technol.* **2024**, *38*, 2103–2122. [CrossRef]

37. González Castillo, I.; Loboda, I. Analysis of Nonlinear Gas Turbine Models Using Influence Coefficients. *Ing. Investig. Y Tecnol.* **2021**, *22*, 1–17. [CrossRef]

38. Vladov, S.; Shmelov, Y.; Yakovliev, R. Helicopters Aircraft Engines Self-Organizing Neural Network Automatic Control System. *CEUR Workshop Proc.* **2022**, *3137*, 28–47. [CrossRef]

39. Sina Tayarani-Bathaie, S.; Sadough Vanini, Z.N.; Khorasani, K. Dynamic Neural Network-Based Fault Diagnosis of Gas Turbine Engines. *Neurocomputing* **2014**, *125*, 153–165. [CrossRef]

40. Vladov, S.; Shmelov, Y.; Yakovliev, R. Modified Helicopters Turboshaft Engines Neural Network Onboard Automatic Control System Using the Adaptive Control Method. *CEUR Workshop Proc.* **2022**, *3309*, 205–224.

41. Vladov, S.; Shmelov, Y.; Yakovliev, R.; Petchenko, M. Modified Neural Network Fault-Tolerant Closed Onboard Helicopters Turboshaft Engines Automatic Control System. *CEUR Workshop Proc.* **2023**, *3387*, 160–179.

42. Vladov, S.; Shmelov, Y.; Yakovliev, R.; Petchenko, M. Neural Network Method for Parametric Adaptation Helicopters Turboshaft Engines Onboard Automatic Control System Parameters. *CEUR Workshop Proc.* **2023**, *3403*, 179–195.

43. Ibrahem, I.M.A.; Akhrif, O.; Moustapha, H.; Staniszewski, M. Nonlinear Generalized Predictive Controller Based on Ensemble of NARX Models for Industrial Gas Turbine Engine. *Energy* **2021**, *230*, 120700. [CrossRef]

44. Vladov, S.; Shmelov, Y.; Yakovliev, R.; Kozlovskaya, T.; Petchenko, M. Helicopters Turboshaft Engines Intelligent Control Algorithms Synthesis, Taking into Account Required Quality Provision. *CEUR Workshop Proc.* **2023**, *3468*, 71–90.

45. Vladov, S.; Scislo, L.; Sokurenko, V.; Muzychuk, O.; Vysotska, V.; Sachenko, A.; Yurko, A. Helicopter Turboshaft Engines' Gas Generator Rotor R.P.M. Neuro-Fuzzy Onboard Controller Development. *Energies* **2024**, *17*, 4033. [CrossRef]

46. Vladov, S.; Yakovliev, R.; Hubachov, O.; Rud, J. Neuro-Fuzzy System for Detection Fuel Consumption of Helicopters Turboshaft Engines. *CEUR Workshop Proc.* **2024**, *3628*, 55–72.

47. Vladov, S.; Bulakh, M.; Vysotska, V.; Yakovliev, R. Onboard Neuro-Fuzzy Adaptive Helicopter Turboshaft Engine Automatic Control System. *Energies* **2024**, *17*, 4195. [CrossRef]

48. Vasiliev, V.; Valeev, S. Design of intelligent control systems for gas turbine engines based on the principle of minimum complexity. *Bull. USATU* **2007**, *9*, 32–41.

49. Pogorelov, G.I.; Kulikov, G.G.; Abdulnagimov, A.I.; Badamshin, B.I. Application of Neural Network Technology and High-Performance Computing for Identification and Real-time Hardware-in-the-Loop Simulation of Gas Turbine Engines. *Procedia Eng.* **2017**, *176*, 402–408. [CrossRef]

50. Vladov, S.; Shmelov, Y.; Yakovliev, R.; Petchenko, M.; Drozdova, S. Neural Network Method for Helicopters Turboshaft Engines Working Process Parameters Identification at Flight Modes. In Proceedings of the 2022 IEEE 4th International Conference on Modern Electrical and Energy System (MEES), Kremenchuk, Ukraine, 20–22 October 2022. [CrossRef]

51. Vladov, S.; Scislo, L.; Sokurenko, V.; Muzychuk, O.; Vysotska, V.; Osadchy, S.; Sachenko, A. Neural Network Signal Integration from Thermogas-Dynamic Parameter Sensors for Helicopters Turboshaft Engines at Flight Operation Conditions. *Sensors* **2024**, *24*, 4246. [CrossRef]

52. Kim, S.; Im, J.H.; Kim, M.; Kim, J.; Kim, Y.I. Diagnostics using a physics-based engine model in aero gas turbine engine verification tests. *Aerosp. Sci. Technol.* **2023**, *133*, 108102. [CrossRef]

53. Vladov, S.; Yakovliev, R.; Hubachov, O.; Rud, J.; Drodova, S.; Perekrest, A. Modified Discrete Neural Network PID Controller for Controlling the Helicopters Turboshaft Engines Free Turbine Speed. In Proceedings of the 2023 IEEE 5th International Conference on Modern Electrical and Energy System (MEES), Kremenchuk, Ukraine, 27–30 September 2023; pp. 797–802. [CrossRef]

54. Vladov, S.; Shmelov, Y.; Yakovliev, R.; Stushchankyi, Y.; Havryliuk, Y. Neural Network Method for Controlling the Helicopters Turboshaft Engines Free Turbine Speed at Flight Modes. *CEUR Workshop Proc.* **2023**, *3426*, 89–108.

55. Catana, R.M.; Dediu, G. Analytical Calculation Model of the TV3-117 Turboshaft Working Regimes Based on Experimental Data. *Appl. Sci.* **2023**, *13*, 10720. [CrossRef]

56. Gebrehiwet, L.; Nigussei, Y.; Teklehaymanot, T. A Review-Differentiating TV2 and TV3 Series Turbo Shaft Engines. *Int. J. Res. Publ. Rev.* **2022**, *3*, 1822–1838. [CrossRef]

57. Vladov, S.; Sachenko, A.; Sokurenko, V.; Muzychuk, O.; Vysotska, V. Helicopters Turboshaft Engines Neural Network Modeling under Sensor Failure. *J. Sens. Actuator Netw.* **2024**, *13*, 66. [CrossRef]

58. Pasieka, M.; Grzesik, N.; Kuźma, K. Simulation modeling of fuzzy logic controller for aircraft engines. *Int. J. Comput.* **2017**, *16*, 27–33. [CrossRef]

59. Marakhimov, A.R.; Khudaybergenov, K.K. Approach to the synthesis of neural network structure during classification. *Int. J. Comput.* **2020**, *19*, 20–26. [CrossRef]

60. Kim, H.-Y. Statistical Notes for Clinical Researchers: Chi-Squared Test and Fisher's Exact Test. *Restor. Dent. Endod.* **2017**, *42*, 152. [CrossRef]

61. Balakrishnan, N.; Voinov, V.; Nikulin, M.S. Chapter 2—Pearson's Sum and Pearson-Fisher Test. In *Chi-Squared Goodness of Fit Tests with Applications*; Balakrishnan, N., Voinov, V., Nikulin, M.S., Eds.; Academic Press: Waltham, MA, USA, 2013; pp. 11–26. [CrossRef]

62. Cosenza, P.; Fauchille, A.-L.; Prêt, D.; Hedan, S.; Giraud, A. Statistical Representative Elementary Area of Shale Inferred by Micromechanics. *Int. J. Eng. Sci.* **2019**, *142*, 53–73. [CrossRef]

63. Avram, F.; Leonenko, N.N.; Šuvak, N. Hypothesis testing for Fisher–Snedecor diffusion. *J. Stat. Plan. Inference* **2012**, *142*, 2308–2321. [CrossRef]

64. Stefanovic, C.M.; Armada, A.G.; Costa-Perez, X. Second Order Statistics of -Fisher-Snedecor Distribution and Their Application to Burst Error Rate Analysis of Multi-Hop Communications. *IEEE Open J. Commun. Soc.* **2022**, *3*, 2407–2424. [CrossRef]

65. Benaceur, A.; Verfürth, B. Statistical Variational Data Assimilation. *Comput. Methods Appl. Mech. Eng.* **2024**, *432*, 117402. [CrossRef]

66. Babichev, S.; Krejci, J.; Bicanek, J.; Lytvynenko, V. Gene expression sequences clustering based on the internal and external clustering quality criteria. In Proceedings of the 2017 12th International Scientific and Technical Conference on Computer Sciences and Information Technologies (CSIT), Lviv, Ukraine, 5–8 September 2017. [CrossRef]

67. Hu, Z.; Kashyap, E.; Tyshchenko, O.K. *GEOCLUS: A Fuzzy-Based Learning Algorithm for Clustering Expression Datasets*; Lecture Notes on Data Engineering and Communications Technologies; Springer: Cham, Switzerland, 2022; Volume 134, pp. 337–349. [CrossRef]

68. Altameem, A.; Al-Ma'aitah, M.; Kovtun, V.; Altameem, T. A Computationally Efficient Method for Assessing the Impact of an Active Viral Cyber Threat on a High-Availability Cluster. *Egypt. Inform. J.* **2023**, *24*, 61–69. [CrossRef]

69. Vlasenko, D.; Inkarbaieva, O.; Peretiatko, M.; Kovalchuk, D.; Sereda, O. Helicopter Radio System for Low Altitudes and Flight Speed Measuring with Pulsed Ultra-Wideband Stochastic Sounding Signals and Artificial Intelligence Elements. *Radioelectron. Comput. Syst.* **2023**, *3*, 48–59. [CrossRef]

70. Rusyn, B.; Lutsyk, O.; Kosarevych, R.; Obukh, Y. *Application Peculiarities of Deep Learning Methods in the Problem of Big Datasets Classification*; Lecture Notes in Electrical Engineering; Springer: Cham, Switzerland, 2021; Volume 831, pp. 493–506. [CrossRef]

71. Rusyn, B.; Lutsyk, O.; Kosarevych, R.; Kapshii, O.; Karpin, O.; Maksymyuk, T.; Gazda, J. Rethinking Deep CNN Training: A Novel Approach for Quality-Aware Dataset Optimization. *IEEE Access* **2024**, *12*, 137427–137438. [CrossRef]

72. Turchenko, V.; Chalmers, E.; Luczak, A. A deep convolutional auto-encoder with pooling–unpooling layers in caffe. *Int. J. Comput.* **2019**, *1*, 8–31. [CrossRef]

73. Komar, M.; Sachenko, A.; Golovko, V.; Dorosh, V. Compression of network traffic parameters for detecting cyber attacks based on deep learning. In Proceedings of the 2018 IEEE 9th International Conference on Dependable Systems, Services and Technologies (DESSERT), Kyiv, Ukraine, 24–27 May 2018; pp. 43–47. [CrossRef]

74. Kovtun, V.; Altameem, T.; Al-Maitah, M.; Kempa, W. Entropy-Metric Estimation of the Small Data Models with Stochastic Parameters. *Heliyon* **2024**, *10*, e24708. [CrossRef]

75. Tverdokhlib, O.; Vysotska, V.; Pukach, P.; Vovk, M. *Information Technology for Identifying Hate Speech in Online Communication Based on Machine Learning*; Lecture Notes on Data Engineering and Communications Technologies; Springer: Cham, Switzerland, 2024; Volume 195, pp. 339–369. [CrossRef]

76. Lytvyn, V.; Dudyk, D.; Peleshchak, I.; Peleshchak, R.; Pukach, P. Influence of the Number of Neighbours on the Clustering Metric by Oscillatory Chaotic Neural Network with Dipole Synaptic Connections. *CEUR Workshop Proc.* **2024**, *3664*, 24–34.

77. Kovtun, V.; Grochla, K.; Połys, K. Investigation of the Information Interaction of the Sensor Network End IoT Device and the Hub at the Transport Protocol Level. *Electronics* **2023**, *12*, 4662. [CrossRef]

78. Nazarkevych, M.; Kowalska-Styczen, A.; Lytvyn, V. Research of Facial Recognition Systems and Criteria for Identification. In Proceedings of the IEEE International Conference on Intelligent Data Acquisition and Advanced Computing Systems: Technology and Applications, IDAACS, Dortmund, Germany, 7–9 September 2023; pp. 555–558. [CrossRef]

79. Gifalli, A.; Bonini Neto, A.; de Souza, A.N.; de Mello, R.P.; Ikeshoji, M.A.; Garbelini, E.; Neto, F.T. Fault Detection and Normal Operating Condition in Power Transformers via Pattern Recognition Artificial Neural Network. *Appl. Syst. Innov.* **2024**, *7*, 41. [CrossRef]

80. Aliyari, M.; Ayele, Y.Z. Application of Artificial Neural Networks for Power Load Prediction in Critical Infrastructure: A Comparative Case Study. *Appl. Syst. Innov.* **2023**, *6*, 115. [CrossRef]

81. Ale Isaac, M.S.; Flores Peña, P.; Gîfu, D.; Ragab, A.R. Advanced Control Strategies for Securing UAV Systems: A Cyber-Physical Approach. *Appl. Syst. Innov.* **2024**, *7*, 83. [CrossRef]

82. Pang, S.; Jafari, S.; Nikolaidis, T.; Li, Q. A Novel Model-Based Multivariable Framework for Aircraft Gas Turbine Engine Limit Protection Control. *Chin. J. Aeronaut.* **2021**, *34*, 57–72. [CrossRef]

83. Kilic, U.; Villareal-Valderrama, F.; Ayar, M.; Ekici, S.; Amezquita-Brooks, L.; Karakoc, T.H. Deep Learning-Based Forecasting Modeling of Micro Gas Turbine Performance Projection: An Experimental Approach. *Eng. Appl. Artif. Intell.* **2024**, *130*, 107769. [CrossRef]

84. Liu, X.; Song, E.; Zhang, L.; Luan, Y.; Wang, J.; Luo, C.; Xiong, L.; Pan, Q. Design and Implementation for the State Time-Delay and Input Saturation Compensator of Gas Turbine Aero-Engine Control System. *Energy* **2024**, *288*, 129934. [CrossRef]

85. Singh, R.; Maity, A.; Nataraj, P.S.V. Dynamic Modeling and Robust Nonlinear Control of a Laboratory Gas Turbine Engine. *Aerosp. Sci. Technol.* **2022**, *126*, 107586. [CrossRef]

86. Zimbrod, P.; Fleck, M.; Schilp, J. An Application-Driven Method for Assembling Numerical Schemes for the Solution of Complex Multiphysics Problems. *Appl. Syst. Innov.* **2024**, *7*, 35. [CrossRef]

87. de Voogt, A.; Amour, E.S. Safety of Twin-Engine Helicopters: Risks and Operational Specificity. *Saf. Sci.* **2021**, *136*, 105169. [CrossRef]

88. de Voogt, A.; Nero, K. Technical Failures in Helicopters: Non-Powerplant-Related Accidents. *Safety* **2023**, *9*, 10. [CrossRef]

89. Aygun, H.; Caliskan, H. Evaluating and Modelling of Thermodynamic and Environmental Parameters of a Gas Turbine Engine and Its Components. *J. Clean. Prod.* **2022**, *365*, 132762. [CrossRef]

90. Xu, M.; Liu, J.; Li, M.; Geng, J.; Wu, Y.; Song, Z. Improved Hybrid Modeling Method with Input and Output Self-Tuning for Gas Turbine Engine. *Energy* **2022**, *238*, 121672. [CrossRef]

91. Yu, Z.; Yan, X.; Chen, R. Prediction of Pilot Workload in Helicopter Landing after One Engine Failure. *Chin. J. Aeronaut.* **2020**, *33*, 3112–3124. [CrossRef]

92. Chi, C.; Yan, X.; Chen, R.; Li, P. Analysis of Low-Speed Height-Velocity Diagram of a Variable-Speed-Rotor Helicopter in One-Engine-Failure. *Aerosp. Sci. Technol.* **2019**, *91*, 310–320. [CrossRef]

93. Mohammed, M.; Taher, M.K.; khudhair, S. Prediction of Turbojet Performance by Using Artificial Neural Network. *Mater. Today Proc.* **2022**, *60*, 1513–1522. [CrossRef]

94. De Giorgi, M.G.; Quarta, M. Hybrid MultiGene Genetic Programming—Artificial Neural Networks Approach for Dynamic Performance Prediction of an Aeroengine. *Aerosp. Sci. Technol.* **2020**, *103*, 105902. [CrossRef]

95. Ma, Y.; Du, X.; Sun, X. Adaptive Modification of Turbofan Engine Nonlinear Model Based on LSTM Neural Networks and Hybrid Optimization Method. *Chin. J. Aeronaut.* **2022**, *35*, 314–332. [CrossRef]

96. Wang, Y.; Huang, J.; Zhou, W.; Lu, F.; Xu, W. Neural Network-Based Model Predictive Control with Fuzzy-SQP Optimization for Direct Thrust Control of Turbofan Engine. *Chin. J. Aeronaut.* **2022**, *35*, 59–71. [CrossRef]

97. Pu, J.; Zhang, Y.; Guan, Y.; Cui, N. Recurrent Neural Network-Based Predefined Time Control for Morphing Aircraft with Asymmetric Time-Varying Constraints. *Appl. Math. Model.* **2024**, *135*, 578–600. [CrossRef]

98. Song, Z.; Feng, Y.; Lu, C. Superimposable Neural Network for Health Monitoring of Aircraft Hydraulic System. *Eng. Fail. Anal.* **2024**, *160*, 108063. [CrossRef]

99. Xiao, D.; Xiao, H.; Li, R.; Wang, Z. Application of Physical-Structure-Driven Deep Learning and Compensation Methods in Aircraft Engine Health Management. *Eng. Appl. Artif. Intell.* **2024**, *136*, 109024. [CrossRef]

100. Zhao, Y.-P.; Huang, G.; Hu, Q.-K.; Tan, J.-F.; Wang, J.-J.; Yang, Z. Soft Extreme Learning Machine for Fault Detection of Aircraft Engine. *Aerosp. Sci. Technol.* **2019**, *91*, 70–81. [CrossRef]

101. Boujamza, A.; Elhaq, S.L. Optimizing Remaining Useful Life Predictions for Aircraft Engines: A Dilated Recurrent Neural Network Approach. *IFAC-PapersOnLine* **2024**, *58*, 811–816. [CrossRef]

102. Zhou, D.; Zhuang, X.; Zuo, H. A Hybrid Deep Neural Network Based on Multi-Time Window Convolutional Bidirectional LSTM for Civil Aircraft APU Hazard Identification. *Chin. J. Aeronaut.* **2022**, *35*, 344–361. [CrossRef]

103. Wei, Z.; Zhao, Z.; Zhou, Z.; Yan, R. Collaborative-Sequential Optimization for Aero-Engine Maintenance Based on Multi-Agent Reinforcement Learning. *Expert Syst. Appl.* **2024**, *247*, 123358. [CrossRef]

104. Razzaghi, P.; Tabrizian, A.; Guo, W.; Chen, S.; Taye, A.; Thompson, E.; Bregeon, A.; Baheri, A.; Wei, P. A Survey on Reinforcement Learning in Aviation Applications. *Eng. Appl. Artif. Intell.* **2024**, *136*, 108911. [CrossRef]

105. Dangut, M.D.; Jennions, I.K.; King, S.; Skaf, Z. Application of Deep Reinforcement Learning for Extremely Rare Failure Prediction in Aircraft Maintenance. *Mech. Syst. Signal Process.* **2022**, *171*, 108873. [CrossRef]

106. Yu, B.; Shen, E.; Huang, Y.; Lu, F. Research on Self-Learning Control Method for Aircraft Engine above Idle State. *Adv. Mech. Eng.* **2016**, *8*, 1687814016653888. [CrossRef]

107. Liu, L.; Song, X.; Zhou, Z. Aircraft Engine Remaining Useful Life Estimation via a Double Attention-Based Data-Driven Architecture. *Reliab. Eng. Syst. Saf.* **2022**, *221*, 108330. [CrossRef]

108. Baranovskyi, D.; Bulakh, M.; Myamlin, S.; Kebal, I. New Design of the Hatch Cover to Increase the Carrying Capacity of the Gondola Car. *Adv. Sci. Technol. Res. J.* **2022**, *16*, 186–191. [CrossRef]

109. Baranovskyi, D.; Myamlin, S.; Bulakh, M.; Podosonov, D.; Muradian, L. Determination of the Filler Concentration of the Composite Tape. *Appl. Sci.* **2022**, *12*, 11044. [CrossRef]

110. Sagin, S.; Madey, V.; Sagin, A.; Stoliaryk, T.; Fomin, O.; Kučera, P. Ensuring Reliable and Safe Operation of Trunk Diesel Engines of Marine Transport Vessels. *J. Mar. Sci. Eng.* **2022**, *10*, 1373. [CrossRef]

111. Sagin, S.V.; Sagin, S.S.; Fomin, O.; Gaichenia, O.; Zablotskyi, Y.; Píštěk, V.; Kučera, P. Use of Biofuels in Marine Diesel Engines for Sustainable and Safe Maritime Transport. *Renew. Energy* **2024**, *224*, 120221. [CrossRef]